# Lateral Pressure Profile, Spontaneous Curvature Frustration, and the Incorporation and Conformation of Proteins in Membranes

Derek Marsh
Max-Planck-Institut für biophysikalische Chemie, Abt. Spektroskopie, Göttingen, Germany

ABSTRACT Lipid-protein interactions are an important determinant of the stability and function of integral and transmembrane proteins. In addition to local interactions at the lipid-protein interface, global interactions such as the distribution of internal lateral pressure may also influence protein conformation. It is shown here that the effects of the membrane lateral pressure profile on the conformation or insertion of proteins in membranes are equivalent to the elastic response to the frustrated spontaneous curvature, $c_o$, of the component lipid monolayer leaflets. The chemical potential of the protein in the membrane is predicted to depend linearly on the spontaneous curvature of the lipid leaflets, just as does the contribution of the protein to the elastic bending energy of the lipid, and to be independent of the hydrophobic tension, $\gamma_{phob}$, at the lipid-water interface. Analysis of the dependence of protein partitioning or conformational transitions on spontaneous curvature of the constituent lipids gives an experimental estimate for the cross-sectional intramembrane shape of the protein or its difference between conformations. Values in the region of 50–110 Å$^2$ are estimated for the effective cross-sectional shape changes on the insertion and conductance transitions of alamethicin, and on the activation of CTP:phosphocholine cytidylyltransferase or rhodopsin in lipid membranes. Much larger values are estimated for the mechanosensitive channel, MscL. Values for the change in intramembrane shape may also be used, together with determinations of lipid relative association constants, to estimate contributions of direct lipid-protein interactions to the lateral pressure experienced by the protein. Changes in chemical potential ~12 kJ mol$^{-1}$ can be estimated for radial changes of 1 Å in a protein of diameter 40 Å.

## INTRODUCTION

Lateral pressure within membranes is thought to contribute to the dependence of protein function on the membrane lipid composition (see, e.g., (1–3)). Whereas the net lateral pressure or tension of a membrane is zero in its equilibrium state (4), the individual component contributions can reach local pressures of several hundred atmospheres or more (5,6). For instance, the equivalence surface pressure between lipid monolayers and bilayers is in the region of 35 mN m$^{-1}$ (7), which is close to the hydrophobic free energy density on exposure of lipid chains to water (8). The distribution of lateral pressure components across the width of the bilayer, i.e., the lateral pressure profile, may therefore be expected to vary considerably with lipid composition, even for tension-free membranes.

Cantor (9–11) has proposed that differences in shape of the lateral pressure profile can account for the dependence of protein conformation on membrane lipid composition, if the shape of the transmembrane cross section of the protein differs between the two conformations (see Fig. 1). A similar reasoning applies to the partitioning of proteins or peptides into membranes. Unfortunately, lipid lateral pressure is not directly accessible experimentally, although theoretical models suggest that the dependence of the transmembrane profile on lipid chain composition is sufficiently large to affect protein conformation (11,12). Molecular dynamics simulations, on the other hand, have provided rather more equivocal results on this point (6). In addition, the difference in intramembranous shape between functionally relevant conformations is not known for most proteins. This and the theoretical difficulties arising from partial cancellation of large contributions to the lateral pressure that are of opposite sign results in considerable uncertainty as to the quantitative significance of the mechanism for lipid control of membrane function that is proposed by Cantor (compare also (13)).

In principle, one experimental parameter that depends on the lateral pressure profile is the spontaneous lipid curvature (14,15). This is a quantity for which there is a considerable amount of data from x-ray diffraction studies of lipid $H_{II}$-phases under dual-solvent stress (16–20). Also, there are numerous studies that demonstrate a dependence of protein insertion or protein activity on spontaneous curvature of nonlamellar forming lipids (21–26).

It is shown here that the approach involving the lateral pressure profile that is used by Cantor (9) is equivalent to considerations of the spontaneous curvature frustration that was introduced by Helfrich (27) and discussed by Gruner (28) in terms of membrane protein function, and is used extensively in the analysis of nonlamellar lipid phases (see, e.g., (16,29,30)). Analysis of existing data in these terms then gives estimates of the intramembranous shape of proteins on membrane insertion and of the change in transmembrane cross-sectional shape involved in functionally significant conformational transitions. The results additionally provide estimates for the likely change in area of the protein-lipid interface and hence on the direct contribution of

*Submitted March 1, 2007, and accepted for publication July 19, 2007.*

Address reprint requests to D. Marsh, Tel.: 49-551-201-1285; E-mail: dmarsh@gwdg.de.

Editor: Thomas J. McIntosh.


0006-3495/07/12/3884/16 $2.00

doi: 10.1529/biophysj.107.107938

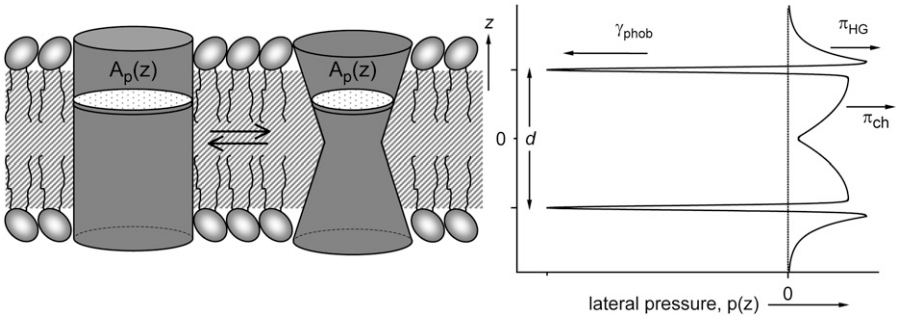


FIGURE 1 Lateral pressure profile, $p(z)$ dz, with distance $z$ from the bilayer mid-plane in a lipid membrane, and the cross-sectional profile, $A_P(z)$, of an inserted transmembrane protein. Integrated contributions of the lipid chains and headgroups to the lateral pressure profile are $\pi_{ch}$ and $\pi_{HG}$, respectively, and $\gamma_{phob}$ is the microscopic hydrophobic interfacial tension contributed by the exposure of the lipid chains to water. The protein is shown schematically in two conformations that differ in the shape of their transmembrane domain.

lipid-protein selectivity to the energetics of different protein conformations.

## Lateral pressure profile

The chemical potential, $\mu_b$, of a protein at mole fraction $X_b$ in the membrane depends on the transmembrane lateral pressure profile, $p(z)\,dz$, according to (9)

$$\mu_b = \mu_b^o + k_B T \ln(X_b) + \int A_P(z)p(z)dz, \qquad (1)$$

where $A_P(z)$ is the cross-sectional area of the protein at distance $z$ from the membrane midplane (see Fig. 1), and other symbols have their usual meaning. The integration in Eq. 1 extends over the full width of the membrane, and the standard chemical potential corresponds to the lateral pressure profile relative to which $p(z)$ is referred. The contribution of the membrane lateral pressure to the change in chemical potential, $\Delta\mu_b$, when a conformational change takes place in the protein is thus given by

$$\Delta\mu_b = \int \Delta A_P(z)p(z)dz, \qquad (2)$$

where $\Delta A_P(z)$ is the difference in cross-sectional area profile of the protein in the two conformations (see Fig. 1, *left*). Equation 2 forms the basis for a mechanism whereby membrane lipid composition, via changes in the lateral pressure profile, may affect the conformational equilibria of integral membrane proteins (9). To be effective, this mechanism requires a marked difference $\Delta A(z)$ in the transmembrane shape of the protein between the two conformations, and it also depends quite critically on the size of the change $\Delta p(z)$ in the lateral pressure profile with lipid composition.

Contributions from the two apposing monolayers of the lipid membrane are additive in Eq. 2. For a symmetrical bilayer, the lateral pressure profile has reflection symmetry about the midplane $z = 0$, i.e., $p(-z) = p(z)$ (see Fig. 1, *right*). Antisymmetric changes in cross-sectional area profile $\Delta A_P(-z) = -\Delta A_P(z)$, e.g., of conical shape, then produce no net change in chemical potential of the protein in a symmetric bilayer. On the other hand, changes in cross-sectional area profile having reflection symmetry $\Delta A_P(-z) = \Delta A_P(z)$, e.g., of hourglass shape (see Fig. 1, *left*), produce a net change in chemical potential, $\Delta\mu_b$, in symmetrical bilayers that is twice that for a single monolayer.

The lateral pressure profile in a bilayer membrane is composed essentially of three contributions (1),

$$p(z) = \pi'_{ch}(z) + \pi'_{HG}(z) - \gamma_{phob}(\delta(z - d/2) + \delta(z + d/2)), \qquad (3)$$

where $\pi'_{HG}(z) \equiv \partial\pi_{HG}(z)/\partial z$ and $\pi'_{ch}(z) \equiv \partial\pi_{ch}(z)/\partial z$ are the repulsive lateral pressure profiles in the lipid headgroup and hydrocarbon chain regions of the membrane, respectively, and $\gamma_{phob}$ is the hydrophobic free energy density (or interfacial tension) for the interaction of the lipid chains with water (see Fig. 1, *right*). The latter acts at the polar-apolar interfaces of the membrane, which are situated at a distance $z = \pm d/2$ from the center of the membrane. In Eq. 3, $\delta(z)$ is the Dirac $\delta$-function, which idealizes the nonvanishing thickness of the polar-apolar interface. However, the effective thickness will be less than that characterized by experimental water penetration profiles (31–36) because the latter is at the level of individual water molecules, whereas the hydrophobic effect requires contact with bulk water for its thermodynamic (entropic) expression (1,8,37). (Note also that molecular dynamics simulations of lateral pressure profiles are frequently characterized by strong negative peaks close to the polar-apolar interfaces; see, e.g., (6)).

For membranes with different lipid compositions, the change in lateral pressure profile is given by

$$\Delta p(z) = \Delta\pi'_{ch}(z) + \Delta\pi'_{HG}(z), \qquad (4)$$

where $\Delta\pi'_{HG}(z)$ and $\Delta\pi'_{ch}(z)$ are the contributions of the lipid headgroup and hydrocarbon chain regions, respectively, to the difference in repulsive lateral pressure profiles. Note that the interfacial hydrophobic free energy density (i.e., $\gamma_{phob}$) does not enter into Eq. 4, because it is characterized by the contact of hydrocarbon with bulk water and therefore is much the same for all lipids (see, e.g., (1,8,37)). For membranes with lateral pressure profiles that differ by an amount $\Delta p(z)$, the difference, $\Delta\Delta\mu_b$, in the change in chemical potential that accompanies a conformational change is given by

$$\Delta\Delta\mu_b = \int \Delta A(z)\Delta p(z)dz. \qquad (5)$$

Thus, from Eq. 4, the sensitivity of the protein conformation to lipid composition is independent of the interfacial tension, $\gamma_{phob}$, of the hydrophobic effect.

The size of the hydrophobic interfacial tension therefore affects protein conformational equilibria only rather indirectly. A membrane in its normal relaxed state is free of tension (1,4). Therefore the integral of the lateral pressure profile across the full width of the membrane must vanish: $\int p(z)dz = 0$. Hence, from Eq. 3, this condition for mechanical equilibrium is (1)

$$2\gamma_{phob} = \int \pi'_{ch}(z)dz + \int \pi'_{HG}(z)dz, \quad (6)$$

and the overall size of the lateral pressure profiles is $\sim\gamma_{phob}/d_m$, which has the dimensions of force per unit area, where $d_m$ is the thickness of a membrane monolayer leaflet. Comparison between lipid monolayers and lipid bilayers indicates that the effective size of the microscopic hydrophobic interfacial energy density is $\gamma_{phob} \sim 35$ mN m$^{-1}$ at the polar-apolar interface of the membrane (1), rather than 50 mN m$^{-1}$, which is found for the macroscopic surface tension of oil-water interfaces (7,38). An order-of-magnitude estimate of the relative size of the headgroup and chain contributions to the internal lateral pressure suggests that $\pi_{HG}/\pi_{ch} \sim 1$ for phosphatidylethanolamines, based on the dimensions of the $H_{II}$-phases (39).

The components of the internal lateral pressure in a membrane and their transmembrane profiles are not accessible to direct measurement because the net lateral pressure in a membrane at equilibrium is zero. To relate the effects of the lateral pressure profile on protein conformational equilibria to experimentally accessible quantities it is necessary to introduce the elastic constants for membrane bending. This includes especially the spontaneous (or intrinsic) curvature (28), but also the bending moduli, because these too are related directly to the lateral pressure profile (14,40,41).

## Moments of the lateral pressure profile

It was pointed out by Cantor (10) that the transmembrane profile of the cross-sectional area of the protein can be expanded in a Taylor series,

$$A_P(z) = A_P(0) + a_{1,P}z + a_{2,P}z^2 + \ldots \quad (7)$$

about the center of the membrane, where $a_{i,P}$ are the expansion coefficients. Then the corresponding contributions to the chemical potential of the protein depend on the moments of the lateral pressure profile,

$$\mu_b = \mu_b^o + k_BT\ln(X_b) + a_{1,P}\int zp(z)dz + a_{2,P}\int z^2p(z)dz + \ldots, \quad (8)$$

where the initial term, $A_P(0)$, in the area expansion does not enter because $\int p(z)dz = 0$.

The moments of the lateral pressure profile can be expressed in terms of the elastic constants for bending (14). The spontaneous bending moment (per unit length) depends on the first moment of the pressure profile and is given simply by

$$k_c c_o = \int zp(z)dz, \quad (9)$$

where $k_c$ is the bending rigidity, or mean-curvature elastic modulus, and $c_o$ is the spontaneous curvature. The first moment does not depend on the choice of the origin for $z$, because $\int p(z)dz = 0$. The elastic modulus for Gaussian curvature, $\bar{k}_c$, is determined by the second moment of the pressure profile (14),

$$\bar{k}_c = -\int (z-\delta)^2 p(z)dz, \quad (10)$$

where $z = \delta$ is the position of the neutral plane. Equations 9 and 10 therefore allow the chemical potential of the protein in Eq. 8 to be rewritten as

$$\mu_b = \mu_b^o + k_BT\ln(X_b) + (a_{1,P} + 2a_{2,P}\delta)k_c c_o - a_{2,P}\bar{k}_c. \quad (11)$$

Equation 11 expresses the contribution from the lateral pressure profile to the chemical potential of the protein in terms of the experimentally accessible quantities, $k_c$, $\bar{k}_c$ and $c_o$. This expansion holds insofar as the profile of the cross-sectional area of the protein can be depicted adequately by the first three terms in Eq. 7. To this level of approximation, the contributions of the membrane lateral pressure profile to the chemical potential of the protein are given by a term that depends linearly on the spontaneous curvature of the lipids, plus a constant.

The parameterization in Eq. 11 involves the position, $\delta$, of the neutral surface, relative to the bilayer midplane. It is usually found that the neutral surface in lipid membranes lies close to the polar-apolar interface (42–44). For the inverted hexagonal phase of dioleoyl phosphatidylethanolamine (DOPE), it is found that the neutral surface lies 0.8 Å below the polar-apolar interface, from the data and expressions given by Leikin et al. (17). For the inverse bicontinuous cubic phase of a monolein, dioleoyl phosphatidylcholine (DOPC) and DOPE mixture, the position of the neutral surface has been determined to be $\delta = 12.9 \pm 0.5$ Å (43). For comparison, the hydrocarbon half-thickness of a DOPC bilayer is $D_c = 13.6 \pm 0.1$ Å (45). Thus a reasonable estimate for membranes of lipids with oleoyl chains is $\delta = 13.5 \pm 1$ Å. The estimated uncertainty in position of the neutral surface will contribute a 7% uncertainty in the upper estimate for the change in contour of the protein (see later).

## Bending elasticity

It is of interest to compare results of the above analysis with those that are obtained from the conventional treatment of

bending elasticity. The elastic free energy of bending for a membrane (or monolayer) surface of area $A$ is given by (27)

$$\Delta G_c(\bar{c}, \bar{c}_G) = \frac{1}{2} k_c A(\bar{c} - c_o)^2 + \bar{k}_c A \bar{c}_G^2, \qquad (12)$$

where the mean (or total) curvature is $\bar{c} = c_1 + c_2$ and the Gaussian curvature is $\bar{c}_G^2 = c_1 c_2$, with $c_1 = 1/R_1$ and $c_2 = 1/R_2$ being the principal curvatures (see Fig. 2). For a flat (i.e., noncurved) reference surface, the elastic free energy is $\Delta G_c(0,0) = (1/2)k_c A c_o^2$, which represents the curvature frustration of the lipids when they are forced into a planar configuration. Thus the chemical potential of a protein in a planar membrane contains a contribution from the change in bending energy of the membrane by introducing the protein, and is given by

$$\mu_b = \mu_b^o + k_B T \ln(X_b) - n_L A_L k_c (\bar{c}_P c_o - \bar{c}_P^2/2 - \bar{k}_c \bar{c}_{G,P}^2/k_c), \qquad (13)$$

where $n_L$ is the number of lipids whose curvature is perturbed by the protein, $A_L$ is the cross-sectional area per lipid molecule, and $\bar{c}_P$ and $\bar{c}_{G,P}$ are the mean and Gaussian curvatures, respectively, of the protein-associated lipids.

As in Eq. 11 above, the contribution of the bending elasticity to the protein chemical potential is linear in the spontaneous curvature, plus a constant term. However, the adaptation of the lipids to the protein surface is expressed differently in the two cases: either in terms of the cross-sectional profile of the protein, or by the change in effective curvature of the lipids. The adaptation of the lipid curvature ($\bar{c}_P$) to the intramembranous shape of the protein (characterized by $a_{1,P}$ and $a_{2,P}$) can be parameterized by comparing the coefficients of the $k_c c_o$ terms in Eqs. 11 and 13. It should be noted that the elastic contribution refers to the alleviation of lipid curvature frustration at the protein surface and includes only implicitly any change in curvature of the actual membrane surface, such as might occur in the case of hydrophobic mismatch between protein and lipid (46,47).

In the analysis of experimental data that is performed later, $n_L$ is taken as the number of lipids in the first boundary shell surrounding the protein (48,49). Thus the values deduced for $\bar{c}_P$ represent the adaptation of the lipid curvature averaged over the first shell of perimeter lipids. If the perturbation of the lipid curvature by the protein extends beyond the first shell (but see (50,51)), then the values of $\bar{c}_P$ that are quoted will represent an upper limit for the first-shell average.

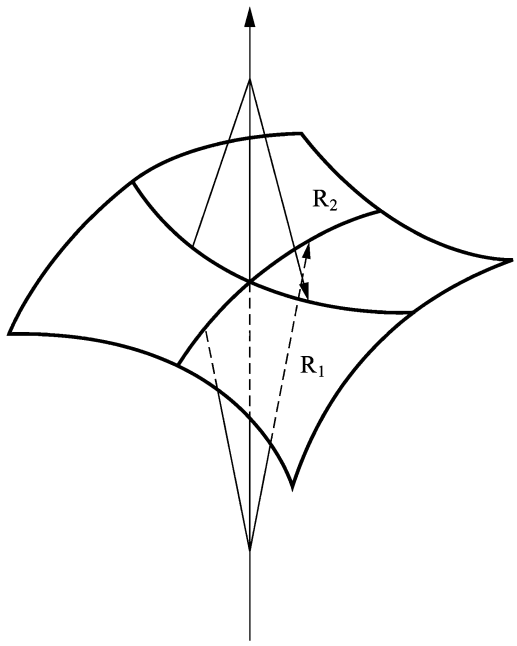


FIGURE 2 Bending of a lipid monolayer with principal curvatures $c_1 = 1/R_1$ and $c_2 = 1/R_2$. The mean curvature is given by $\bar{c} = c_1 + c_2$ and the Gaussian curvature is given by $\bar{c}_G^2 = c_1 c_2$. For cylindrical bending, $\bar{c} = c_1$ and $\bar{c}_G = 0$, and for a spherical vesicle/micelle, $\bar{c}/2 = c_1 = c_2 = \bar{c}_G$.

## Spontaneous curvature

The spontaneous or intrinsic curvature of a monolayer can be parameterized in terms of the volume, $V$, and the effective length, $l$, and cross-sectional area, $A_L$, of the constituent lipid molecules. For a cylindrical system, i.e., $c_2 = 0$ and $\bar{c} = c_1$, the spontaneous curvature in Eq. 12 is given by (52)

$$c_o = \frac{1}{R_{1,o}} = \frac{2}{l}\left(1 - \frac{V}{A_L l}\right), \qquad (14)$$

where $R_{1,o}$ is the spontaneous radius of curvature as normally measured in fully hydrated $H_{II}$ lipid phases in the presence of excess hydrocarbon (see Fig. 3). Here, outward curvatures (oil-in-water; $V/A_L l < 1$) are defined as positive and inward curvatures (water-in-oil; $V/A_L l > 1$) as negative. Equation 14 is purely geometrical and applies to any choice of dividing surface, including the pivotal plane or the neutral surface (17,53). The volume $V$ and length $l$ then refer to that portion of the lipid that lies within the plane (for positive curvatures), or outside the plane (for negative curvatures).

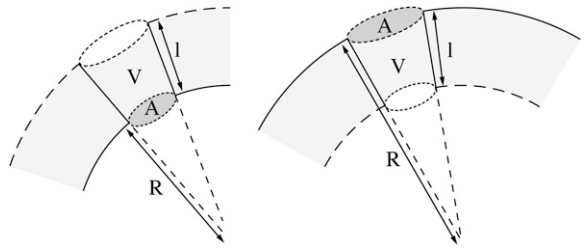


FIGURE 3 Topology of (*right*) normal (oil-in-water) and (*left*) inverted (water-in-oil) curved lipid monolayers, indicating the characteristic dimensions: volume $V$, length $l$, and cross-sectional area $A_L$, of a lipid molecule that specify the monolayer curvature $\pm 1/R$ (*upper* and *lower signs* for *right* and *left*, respectively). The surface to which $R$ is measured is taken as the lipid-water interface, but an alternative definition is to take the neutral or pivotal plane, with corresponding redefinition of the characteristic lipid dimensions.

A sum rule can be given for the spontaneous curvatures of lipid mixtures (A and B) that is based on the conservation of the lipid volumes, $V_A$ and $V_B$,

$$V = V_A X_A + V_B X_B, \tag{15}$$

where $X_A$ and $X_B$ are the mole fractions of lipids A and B, respectively, and the additivity of the lipid areas, $A_A$ and $A_B$,

$$A_L = A_A X_A + A_B X_B, \tag{16}$$

at the dividing surface. In the case of lipids of different lengths or chain compositions, it is necessary also to assume linear additivity of the lipid lengths, $l_A$ and $l_B$:

$$l = l_A X_A + l_B X_B. \tag{17}$$

This approach, by substituting Eqs. 15–17 in Eq. 14, is demonstrated to work for mixtures of DOPE with DOPC (52), and of DOPE with dioleoyl glycerol (53). In the latter two cases, linear additivity of the component spontaneous curvatures, $c_{o,A}$ and $c_{o,B}$,

$$c_o = c_{o,A} X_A + c_{o,B} X_B, \tag{18}$$

is also found to be a reasonable approximation (17), as is illustrated in Fig. 4. For mixtures of DOPC with cholesterol, however, there are marked deviations from Eq. 18 (18). Values for the spontaneous curvature of $(c_o^{DOPE} - c_o^{DOPC}) = -(0.0365 \pm 0.0021)$ Å$^{-1}$ and $c_o^{DOPE} = -0.0431 \pm 0.0009$ Å$^{-1}$ are deduced from the linear regression for DOPE-DOPC mixtures in Fig. 4. The quantity required for the subsequent analysis is $c_o^{DOPE} - c_o^{DOPC}$, which would contribute a 6% uncertainty to the final values deduced from Eqs. 11 or 13.

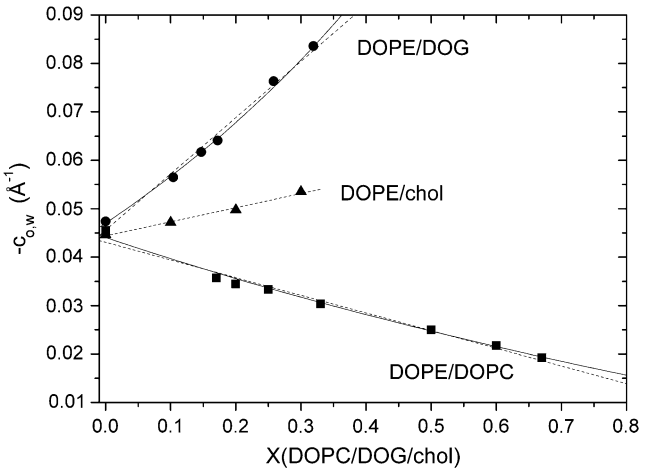


FIGURE 4 Spontaneous curvature, $c_{o,w}$, of the lipid-water interface in fully hydrated lipid mixtures with DOPE, as a function of the mole fraction, $X$, of the second lipid component. (*Squares*) DOPE and DOPC, in the presence of tetradecane (data from (16)). (*Circles*) DOPE and dioleoyl glycerol (DOG), in the presence of tetradecane (data from (17)). (*Triangles*) DOPE and cholesterol (chol), in the presence of tetradecane (data from (18)). Solid lines are fits of Eqs. 14–17 (52,53), and dashed lines are linear regressions according to Eq. 18.

Where appropriate, however, better precision can be achieved by using the calibration that is based on Eqs. 14–17.

Equations 11 or 13 for the chemical potential of the protein, together with the linear approximation of Eq. 18, therefore offer a viable explanation for the linear dependence of various functional activities on lipid curvature (21,22,25,54). The precondition is that the elastic bending moduli not be very dependent on lipid composition; this is considered in the next section.

## Elastic bending moduli

The bending rigidity, or mean curvature modulus, can be related to the first moment of the lateral pressure profile of the bent monolayer (40):

$$k_c = -\int \frac{\partial p(z)}{\partial \bar{c}} z dz. \tag{19}$$

For a linear lateral pressure distribution, the result for a monolayer is (55)

$$k_c = \frac{1}{12} K_A d_m^2, \tag{20}$$

where $K_A$ is the elastic modulus for area dilation of the monolayer and $d_m$ is the monolayer thickness. An extensive series of measurements on bilayer giant vesicles of different phosphatidylcholines (42) has demonstrated a linear dependence of $(k_c/K_A)^{1/2}$ on the bilayer thickness, $d_t$, according to Eq. 20, with the exception of lipids with polyunsaturated chains that have anomalously low bending rigidities. Further, the elastic expansion modulus, $K_A$, was found not to vary appreciably with lipid chain length. Various measurements of $k_c$ for a lipid monolayer by dual solvent stress in $H_{II}$-phases have yielded a mean value of $(4.5 \pm 0.5) \times 10^{-20}$ J for DOPE (e.g., 19), a value of $4 \times 10^{-20}$ J for DOPC (18), and a similar value of $4 \times 10^{-20}$ J for 30 mol % dioleoyl phosphatidylserine in DOPE (20). Thus differences in lipid headgroup do not appear to have a large influence on the bending modulus.

Using a similar continuum model to that used to obtain Eq. 20 yields the following result for the Gaussian curvature modulus (see, e.g., (56)):

$$\bar{k}_c = -(1 - \sigma)k_c, \tag{21}$$

where $\sigma$ is Poisson's ratio. Assuming volume incompressibility results in the maximum value of $\sigma$ (i.e., $\sigma \leq 0.5$), which therefore yields $\bar{k}_c/k_c \leq -0.5$. Experimental estimates for three different fluid phospholipid systems produce a consistent mean value of $\bar{k}_c/k_c = -(0.80 \pm 0.05)$ (43,44,57).

For further discussion and tabulation of elastic curvature constants of lipid monolayers and bilayers, see Marsh (58). From the more recent measurements that are compiled in the latter reference, a mean value of $k_c = (9.9 \pm 0.6) \times k_B T$ ($N = 10$) can be deduced for monolayers of both DOPE and DOPC. This value for the mean curvature modulus will be

used throughout. It contributes an uncertainty of ~6% to the data for the protein shape/lipid curvature that are deduced below by using Eqs. 11 or 13.

Use of the elastic moduli and spontaneous curvatures determined in pure lipid systems requires that the lipid/protein ratio is sufficiently high that the protein is dispersed in an environment that displays the properties of bulk lipid. There is abundant evidence from electron paramagnetic resonance (EPR) of spin-labeled lipids that this is the case in many natural and reconstituted membranes, and that this bilayer environment interfaces directly with the protein boundary lipid (50,59–64).

## Alamethicin in membranes of mixed lipids

As an example, Fig. 5 gives the dependence of the aqueous-membrane partitioning of spin-labeled alamethicin on lipid composition of DOPC-DOPE mixed bilayers. The peptide is expected to remain in the monomeric state in the absence of a membrane potential (65,66). It was shown by Lewis and Cafiso (22) that the free energy of transfer from the aqueous phase depends linearly on the mole fraction of DOPE and thus is linearly dependent also on the membrane curvature. The solid line in Fig. 5 is the corresponding least-squares fit to the dependence of the partition coefficient, $K_P$, on lipid composition,

$$K_P = \frac{X_b}{X_w} = K_o \exp\left(-b\,\frac{k_c}{k_B T}\,X(\mathrm{DOPE})\right), \qquad (22)$$

where $X_b$ and $X_w$ are the mole fractions of alamethicin in the membrane and in water, respectively, and $K_o$ and $b$ are constants. Equation 22 is consistent with the expression for the chemical potential given by Eq. 11 or 13, if it is assumed that the membrane curvature is linearly dependent on the mole fraction, $X$(DOPE), of DOPE according to Eq. 18, and that the bending rigidity remains approximately constant because DOPE and DOPC have the same chain composition (see Eq. 20 above).

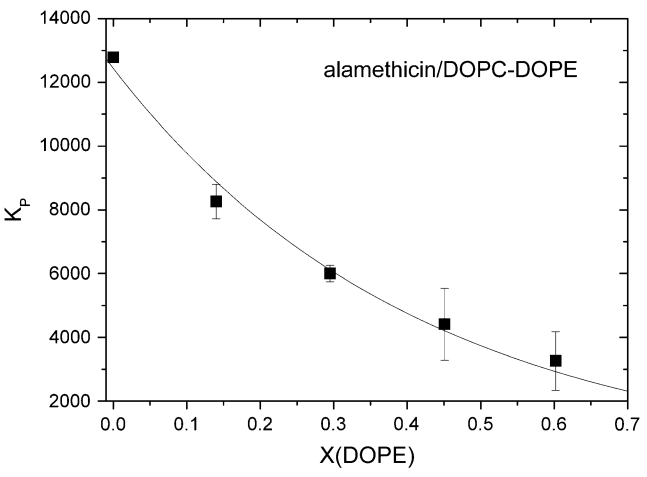


FIGURE 5 Partition coefficient, $K_P$, of alamethicin into membranes of DOPC/DOPE mixtures as a function of the mole fraction, $X$(DOPE), of DOPE (data from (22)). Solid line is a nonlinear least-squares fit of Eq. 22.

A somewhat more precise fitting of Eq. 11 or 13 is obtained, however, by using the calibration for the spontaneous curvatures of DOPC-DOPE mixtures that is based on Eqs. 14–17. Using this data from Fig. 4 and the value given above for $k_c$, it is then estimated that $a_{1,P} + 2a_{2,P}\delta \equiv -n_L A_L \bar{c}_P \approx -7.5 \pm 1.1$ Å. This estimate includes both the uncertainty from fitting the dependence of $K_P$ on $c_o$ and that in $k_c$. For a transmembrane $\alpha$-helix such as alamethicin, the number of first-shell lipids is $n_L \approx 10$–$12$ (48) and the area/lipid for DOPE and DOPC is $A_L \approx 58$–$72$ Å$^2$ (45,52), which yield an effective value of $\bar{c}_P \approx +0.011 \pm 0.004$ Å$^{-1}$ (normal curvature) for the peptide-induced lipid curvature (including uncertainties in $n_L$ and $A_L$). This positive value is reasonable for lipids interacting with a bent $\alpha$-helix that is thought to be almost too short to span the bilayer (22,67), in comparison with spontaneous curvatures of $c_o \approx -0.007$ Å$^{-1}$ and $-0.043$ Å$^{-1}$ (inverted curvature) for DOPC and DOPE, respectively (see Fig. 4). A bent helix is more likely to induce curvature than is a straight helix, and a short helix will provide more space for bulky lipid headgroups, which will tend to favor positive curvature.

Unfortunately, the parameters $a_{1,P}$ and $a_{2,P}$ that govern the transmembrane shape of the protein cannot be determined separately. However, the quantity $a_{1,P}\delta + 2a_{2,P}\delta^2 \approx -100 \pm 20$ Å$^2$ (assuming $\delta \approx 13.5 \pm 1$ Å) provides an upper estimate for the magnitude of the effective difference, $A_P(\delta) - A_P(0)$, in cross-sectional area of the peptide between the membrane midplane and the neutral plane (see Eq. 7). This value is somewhat larger than the cross-sectional area of a phospholipid, and is comparable to that of an $\alpha$-helix. It is probably related, at least in part, to the pronounced kink between the two helical segments of alamethicin (68). In larger peptide/protein assemblies, this value also suggests the order of magnitude likely for realistic changes in cross-sectional area, on conformational changes in the protein.

Keller et al. (21) have performed single-channel conductance measurements on alamethicin in planar-bilayer membranes composed of mixed lipids. Alamethicin ion channels switch between discrete conductance states with jumps in conductance that increase almost linearly with the conductance level. The relative occupancies of successive conductance states, $p_i/p_1$, were found to depend on lipid composition, with an approximately linear dependence of $\ln(p_i/p_1)$ on mole fraction of DOPE in DOPC-DOPE mixtures and hence on spontaneous curvature of the constituent lipid monolayers in accordance with Eq. 11 or 13. From the data of Keller et al. (21), the free energy of the $i^{th}$ conductance level, relative to the first level, $\Delta G_i - \Delta G_1$, then depends linearly on spontaneous curvature of the lipid with gradients of $\sim 59 \pm 8\ k_B T \times$ Å and $130 \pm 9\ k_B T \times$ Å for $i = 2$ and $i = 3$, respectively (see also (69)).

It therefore follows immediately from Eqs. 11 and 13 that the ratio of the differences in $a_{1,P} + 2\delta a_{2,P}$, or in the $n_L\bar{c}_P$ products for the channel-associated lipids, in the two conductance states is $\sim$2.2 $\pm$ 0.2. This is consistent with conductance levels $i = 2$ and $i = 3$ being derived from level $i = 1$ by incorporation of one and two monomers, respectively, in the channel assembly.

It is interesting that the relative populations of channel conductance states, $p_i/p_1$, have the opposite dependence on lipid composition to that of the partitioning of alamethicin into the membrane. From the gradient with respect to lipid spontaneous curvature, it is estimated that the change in $(a_{1,P} + 2a_{2,P}\delta) \equiv -n_L A_L \bar{c}_P$ is $\sim$+6.0 $\pm$ 1.2 Å for the population of the $i = 2$ conductance level, relative to $i = 1$. This corresponds to a negative change in the effective curvature of the channel-associated lipids, on transition to the higher conductance states. Changes in conductance therefore occur via molecular rearrangements within the membrane and not via partitioning of alamethicin from the aqueous phase. An upper estimate for the change in cross-sectional area of the channel at the neutral surface, relative to that at the bilayer midplane, is $\Delta(a_{1,P} + 2\delta a_{2,P}) \times \delta \approx 80 \pm 20$ and 180 $\pm$ 35 Å$^2$ for the $i = 2$ and $i = 3$ conductance levels, respectively. This is comparable in magnitude to the change in internal cross-sectional area on adding one or two monomers, respectively, to the channel assembly.

The effective lipid curvature imposed by the alamethicin channel can be estimated by using the monomer reference state from the partitioning results above, where the gradient of transfer free energy with respect to lipid spontaneous curvature is –74 $\pm$ 6 $k_BT \times$ Å. This yields a value of $-n_L A_L \bar{c}_P \approx$ –(1.6 $\pm$ 1.1) Å for a monomer in the channel assembly. For a regular polygonal arrangement of 6–8 transmembrane $\alpha$-helices, the number of perimeter lipids per monomer is $n_L \approx 3.5 \pm 0.2$ (48,70). Hence, the effective curvature induced by the alamethicin channel is $\bar{c}_P \approx +0.007 \pm 0.006$ Å$^{-1}$. This relatively small value is compatible with a symmetrical arrangement of helices that are bent slightly.

It should be noted that both the partitioning of alamethicin monomers (22) and the populations of alamethicin channel states (21) were also studied with membranes composed of mixtures of *N*-methyl DOPE (DOPE-Me) and DOPC. The spontaneous curvature of DOPE-Me has been measured and lies between that of DOPE and DOPC (71). In both studies, it was found that results similar to those with DOPE-DOPC mixtures were obtained with (DOPE-Me)-DOPC mixtures that had the same value of $c_o$. This shows that spontaneous curvature, rather than chemical composition, is the controlling factor.

## Activation of CTP:phosphocholine cytidylyltransferase

CTP:phosphocholine cytidylyltransferase (CCT) is an enzyme that is involved in lipid biosynthesis and is activated by binding to lipid membranes. Studies on the activation reveal a dependence on lipid composition that implicates spontaneous curvature as a controlling factor (24,72). Attard et al. (24) already have interpreted the dependence of CCT activity on DOPE content of DOPC-DOPE membranes quantitatively in terms of Eq. 13, with spontaneous curvatures of the lipid mixtures predicted by Eq. 18.

Fig. 6 shows the dependence of the chemical potential of membrane-bound CCT on lipid composition, for mixtures of DOPC with DOPE or with dimyristoyl phosphatidylcholine (DMPC). The chemical potential, $\Delta\Delta\mu_b$, relative to a DOPC membrane, is deduced from the activity measurements of Attard et al. (24) by assuming that activation requires binding to the lipid membrane. The linear dependences in Fig. 6 are consistent with a contribution from spontaneous curvature of the lipids that is given by Eq. 11 or 13 and Eq. 18. Using the data of Fig. 4 for DOPE-DOPC mixtures to fit the dependence on $c_o$ directly yields a value of $a_{1,P} + 2a_{2,P}\delta \equiv -n_L A_L \bar{c}_P \approx +3.5 \pm 1.0$ Å. The length of the binding domain of CCT is $\approx$78 $\pm$ 4 Å (24), which suggests that $n_L \approx 16 \pm 1$ lipids are perturbed, yielding a value of $\bar{c}_P \approx -0.0035 \pm 0.0015$ Å$^{-1}$ for the (inverted) curvature of the lipids perturbed by the protein. This value is in reasonable agreement with the original analysis by Attard et al. (24). Alternatively, an upper estimate for the difference, $A_P(\delta) - A_P(0)$, in effective cross-sectional area of the penetrant section of the protein between the membrane midplane and the neutral plane is $a_{1,P}\delta + 2a_{2,P}\delta^2 \approx +47 \pm 16$ Å$^2$ (with $\delta \approx 13.5 \pm 1$ Å).

Measurements of spontaneous curvature are not available for DMPC, but the results of Fig. 6 demonstrate that, unlike for DOPC, this must be of the opposite sign to that for DOPE. It is also possible that differences in bending rigidity between DMPC and DOPC may contribute to the dependence on lipid composition that is shown in Fig. 6. Experimental

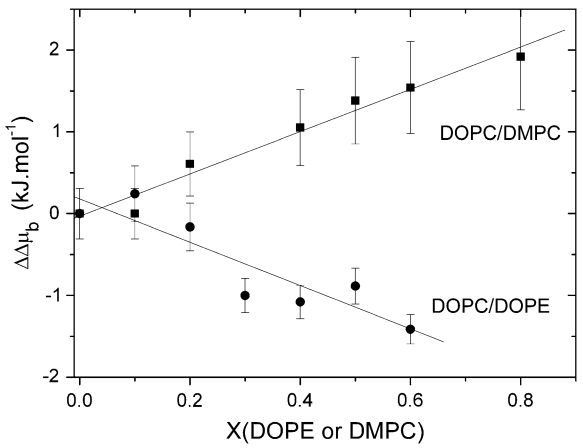


FIGURE 6 Chemical potential, $\Delta\mu_b$, of CTP:phosphocholine cytidylyltransferase bound to membranes of DOPC containing mole fraction, *X*, of DOPE (*circles*) or DMPC (*squares*). Values are obtained from activity measurements, relative to those of the enzyme associated with DOPC alone (data from (24)). Solid lines are linear regressions.

results for bilayers yield values of $k_c = 0.56 \pm 0.06$ and $0.85 \pm 0.10 \times 10^{-19}$ J for DMPC and DOPC, respectively (42). However, the bilayer thickness, $2d_m$, of DMPC does not differ very greatly from that of DOPC (see Eq. 20) (73). Also the lack of a quadratic component to the essentially linear dependence on mole fraction of DMPC in Fig. 6 suggests that differences in bending rigidity do not play a major role. Assuming this to be the case, the ratio of gradients in Fig. 6 gives the following estimate for the spontaneous curvature of DMPC: $c_o \approx +0.03 \pm 0.01$ Å$^{-1}$. This is a lower estimate because it ignores the differences in bending rigidity, but it emphasizes that DMPC, unlike DOPC, strongly favors the formation of phases with normal rather than inverted curvature. A geometrical prediction of the spontaneous curvature for DMPC can be made from Eq. 14, if it is assumed that $l = 15.5$ Å, which is characteristic of the $H_{II}$-phases of DOPE-DOPC mixtures in excess tetradecane (52). The justification for doing this is, as noted above, that DOPC and DMPC have rather similar lipid lengths in the bilayer state. Taking bilayer values of $A_L = 59.6$ Å$^2$ and $V = 1101$ Å$^3$ for DMPC (73) then yields $c_o \approx +0.025$ Å$^{-1}$ from Eq. 14. This is of a similar magnitude to the estimate made above and reflects the expectation that DMPC favors positive curvature, in comparison to DOPE. That lipids with spontaneous intrinsic curvatures of opposite signs respectively decrease and increase the membrane association of CCT is a diagnostic indicator that lipid curvature is involved.

## Meta-I to Meta-II transition in rhodopsin

The meta-I to meta-II state equilibrium of rhodopsin that is reconstituted in mixtures of DOPE with DOPC has been studied by Botelho et al. (25). This MI-MII transition constitutes the primary activation step of the G-protein coupled receptor rhodopsin in visual transduction. It is of particular interest in the context of lipid spontaneous curvature because the MI-MII conformational change leading to activation of G-protein occurs in the membrane-bound protein, as opposed to activation by binding to the membrane. The endogenous lipid of the rod outer segment disc, which is the native environment of rhodopsin, is characterized by a high proportion of poly-unsaturated chains with potentially large spontaneous curvature. Botelho et al. (25) demonstrated a linear dependence of the free energy of the MI-MII transition on spontaneous curvature in DOPC-DOPE mixtures. From the gradient of this dependence, it can be deduced that $\Delta(a_{1,P} + 2a_{2,P}\delta) \equiv -\Delta(n_L A_L \bar{c}_P) = +8.3 \pm 1.2$ Å, according to Eqs. 11, 13, and 18. The number of first-shell lipids associated with bovine rhodopsin has been determined by spin-label EPR to be $n_L \approx 23 \pm 2$ (61,74–76). Thus, the change in the effective mean spontaneous curvature of these lipids associated with rhodopsin is estimated to be $\Delta\bar{c}_P \approx -0.006 \pm 0.002$ Å$^{-1}$. A negative effective spontaneous curvature is expected from the intramembranous shape of rhodopsin (77). An upper estimate for the effective change in transmembrane cross-sectional shape of rhodopsin is given correspondingly by $\Delta(a_{1,P} + 2a_{2,P}\delta) \times \delta \approx +112 \pm 25$ Å$^2$ (with $\delta = 13.5 \pm 1$ Å). This is of the order of magnitude surmised already from the data on alamethicin to be involved in a conformational change of a transmembrane protein. The change in shape on conformational change of a helix bundle could be on the order of a few multiples of the shape asymmetry of a whole helix. For comparison, it is found that the meta-I to meta-II transition is accompanied by a change in volume of rhodopsin of 180 Å$^3$ (78), but this does not exclude larger changes in cross-sectional area that are compensated by changes in thickness of the protein. Also, this volume change includes differences in hydration that could be a major contribution and will mostly affect the extramembranous section of the protein.

From the crystal structure of rhodopsin, the following data, which are in essential agreement with the deductions above regarding the intramembranous shape, may be deduced. The transmembrane domain in the dark state of rhodopsin is roughly elliptical in cross-section with dimensions $\sim 45 \times 37$ Å (79). Thus, the overall cross-sectional area in the plane of the membrane is $\sim 1300$ Å$^2$. The intramembranous protein surface is molecularly rough, but the average tendency of the transmembrane profile resembles the hourglass shape on the left of Fig. 1, as deduced from the accessible surface/perimeter (77). This is because the transmembrane helices of rhodopsin, although bent, are tilted relative to the membrane normal with a crossing that lies within the membrane. Precise quantitation of area profiles in terms of simplified/idealized shapes is, however, difficult.

## Mechanosensitive channel MscL

The prokaryotic mechanosensitive channel of large conductance, MscL, opens in response to membrane tension as a means for combating hypoosmotic stress. Consequently, the protein undergoes a rather large conformational change on channel gating which opens a transmembrane pore with a diameter in the region of 30 Å (80). Moe and Blount (81) have investigated the response to membrane tension in the opening of the MscL channel when it is reconstituted in mixtures of DOPC with DOPE. Although the data consist of only three points, the tension ($T_{1/2}$) for 50% probability of channel opening increases linearly with mole fraction, $X$, of DOPE in the membrane, with a gradient of $\partial T_{1/2}/\partial X = 8.3 \pm 0.5$ mN m$^{-1}$ (81). The free energy of channel gating is related linearly to the value of $T_{1/2}$: $\Delta G = T_{1/2}\Delta\bar{A}_P$, where $\Delta\bar{A}_P = 650$ Å$^2$ for MscL is the increase in mean cross-sectional area of the channel on opening (80). Therefore, the free energy of the open state depends approximately linearly on lipid spontaneous curvature.

From Eqs. 11 and 13 combined with the above data (and Fig. 4), the opening of the MscL channel is predicted to be accompanied by a change in shape that is characterized by a value of $\Delta(a_{1,P} + 2a_{2,P}\delta) \equiv -\Delta(n_L A_L \bar{c}_P) = -44 \pm 3$ Å. An upper estimate for the change in cross-sectional area at the

neutral plane relative to the membrane midplane is therefore $\Delta(a_{1,P} + 2a_{2,P}\delta) \times \delta \approx -595 \pm 90$ Å$^2$, for $\delta = 13.5 \pm 1$ Å. This rather large difference (for a pentameric structure consisting of 10 transmembrane helices; see (82)) is comparable in size to the cross-sectional area of the open pore. It is much larger than in the other examples of conformational shape changes that are considered here and is likely to be a special feature of this particular type of channel.

The MscL channel can be gated by external addition of lysophosphatidylcholine (lysoPC) (83,84). However, in contrast to the effect of phosphatidylethanolamine, the mechanism is thought to involve membrane curvature stress that is induced by asymmetrical incorporation of the lysolipid. When incorporated uniformly in the lipid bilayer, lysoPC failed to induce the conformational signatures in spin-label EPR that are characteristic of the open channel (84). Nonetheless, symmetrically incorporated DOPE was shown to be antagonistic to the effect of asymmetrically incorporated lysoPC. With the eukaryotic mechanosensitive channel TREK-1 in COS cells, arachidonic acid (which likely flip-flops rapidly) induces opening when added to either side of the membrane, whereas lysoPC was only maximally active when added externally to whole cells (85).

Recently, Schmidt et al. (86) have examined the effect of replacing 1-palmitoyl-2-oleoyl phosphatidylethanolamine (POPE) by 1-palmitoyl-2-oleoyl phosphatidylcholine (POPC), on the voltage gating of the KvAP potassium channel in planar bilayer membranes. The midpoint potential for activation changes from $V_{1/2} = -42$ mV in membranes of POPE: POPG 3:1 to $V_{1/2} = -30.5$ mV in membranes of POPC: POPG 3:1, and the valence of the gating charge changes correspondingly from $Z = 3.1$ to $Z = 1.8$ (POPG is 1-palmitoyl-2-oleoyl phosphatidylglycerol). Therefore, the free energy of the open channel state, $\Delta G = ZeV_{1/2}$ (where $e$ is the electronic charge), changes by 7.3 kJ mol$^{-1}$ on replacing POPE by POPC. This is less than that of replacing DOPC by DOPE on gating of MscL ($\delta\Delta G = 32$ kJ mol$^{-1}$), but is comparable in magnitude to that in the other examples of the effects of lipid spontaneous curvature that are considered here. Unfortunately, POPC content relative to POPE was not varied to check whether gating followed the expected dependence on $c_o$. If it is assumed that $c_o$ (and $k_c$) for POPE is similar to that for DOPE, and that for POPC and POPG is similar to that for DOPC, then the change in free energy of gating could be accounted for by a change in protein shape/lipid curvature of $\Delta(a_{1,P} + 2a_{2,P}\delta) \equiv -\Delta(n_L A_L \bar{c}_P) \approx 11 \pm 1$ Å. This would translate to a maximum change in cross-sectional shape of $\Delta(a_{1,P} + 2a_{2,P}\delta) \times \delta \sim 150 \pm 30$ Å$^2$ (for $\delta = 13.5 \pm 1$ Å).

## Energetics of lipid-protein interaction—excess pressure across curved interfaces

The above treatments, in terms either of the lateral pressure profile or of bending elasticity, refer essentially to properties of an unperturbed membrane in which the protein is embedded. This is made especially evident by the quantitation in terms of the curvature elastic constants, $k_c$, $\bar{k}_c$, and $c_o$, of hydrated lipid phases. An alternative, or complementary, approach is to consider directly the energetics of the lipid-protein interface, for which a certain amount of quantitative information is available, particularly from spin-label EPR and fluorescence studies (see, e.g., (59,87–89)). A first approach in this direction was made by Baldwin and Hubbell (90), in terms of the pressure difference across a curved surface that arises from the interfacial tension or excess surface free energy. In this particular context, the authors were considering specifically rhodopsin reconstituted in different lipids.

Let $g_{LP}(z)$ be the excess free energy of interaction per unit area of lipid-protein interface at distance $z$ from the membrane midplane. The appropriate reference state for the lipid-protein interaction, in this case, is the free energy of interaction between lipid molecules in the protein-free membrane. At depth $z$ in the membrane, the cross-sectional area of the protein is $A_P(z) = \pi r_P(z)^2$ and the transmembrane profile of the free energy of lipid-protein interaction is $\Delta G_{LP}(z)dz = 2\pi r_P(z) g_{LP}(z) dz$, where $r_P(z)$ is the radius of the cross-section of the protein at vertical position $z$ in the membrane. Therefore the effective lateral pressure that arises from this interaction is given by

$$p_{LP}(z) = -\frac{\partial \Delta G_{LP}}{\partial A_P} = -\frac{g_{LP}(z)}{r_P(z)}, \tag{23}$$

which is the usual expression (i.e., the Laplace equation) for the excess pressure across a cylindrical surface. For positive $g_{LP}$, the pressure is directed outward from the protein rather than inward from the lipid. Substituting Eq. 23 in Eq. 2 then yields the expected result that the change in chemical potential, $\Delta\mu_b$, when a conformational change takes place in the protein, is given simply by the product of the excess free energy density of the lipid-protein interaction and the change in area of the lipid-protein interface,

$$\Delta\mu_b = -2\pi \int g_{LP}(z) \Delta r_P(z) dz, \tag{24}$$

where $\Delta r_P(z)$ is the difference in profile of the cross-sectional radius of the protein in the two conformations. As might be anticipated, this expression cannot be cast in terms of the bending elasticity of a lipid bilayer, because it refers to the energetics of the lipid-protein interaction.

The profile of the free energy density, $g_{LP}(z)$, can be partitioned into contributions from the lipid headgroups and the lipid chains, as was done for the lateral pressure profile (compare with Eqs. 3 and 4). A term involving the exposure of hydrophobic groups to water ($\gamma_{phob}$) enters only in the case of mismatch between the transmembrane hydrophobic spans of lipid and protein. Conformational changes can be effected by differences in the free energy density profile of lipid-protein interaction, which depend on lipid composition of the host membranes. The excess free energy of interaction with the lipid chains has been measured to be $320 \pm 20$ J mol$^{-1}$ per

$CH_2$ group (per chain) for dark-adapted rhodopsin reconstituted in disaturated phosphatidylcholines (76) and approximately half this for the SERCA $Ca^{2+}$-ATPase reconstituted in 9-*trans*-monounsaturated phosphatidylcholines ((91); see (59)). These values correspond to a contribution from the chains to the excess free energy density of lipid-protein interaction of $g_{LP}^{(ch)} \approx 30$ to 60 J mol$^{-1}$ per Å$^2$ (or 5 to 10 mN m$^{-1}$), assuming a transverse area per $CH_2$ group of 5.3–6.1 Å$^2$ (see, e.g., (92)). Relative association constants of phospholipid species with different polar headgroups typically lie in the range $K_r \approx 0.5$–7, corresponding to differential free energies of lipid-protein interaction of $\sim+2$ to $-5$ kJ mol$^{-1}$, relative to phosphatidylcholine (59,64,93–95). These values are more difficult to translate reliably into an effective excess free energy density than are those for methylene groups. Assuming an effective transverse area per lipid headgroup of $\sim$85 Å$^2$ (see (96)) yields estimates of $\Delta g_{LP}^{(HG)} \approx +20$ to $-60$ J mol$^{-1}$ per Å$^2$ (or $+3$ to $-10$ mN m$^{-1}$) for the average contribution of the lipid polar groups to the excess interaction free energy density, relative to phosphatidylcholine.

From the analysis given above of the functional dependences on lipid spontaneous curvature for alamethicin or CCT, variations in protein cross-sectional area with depth in the membrane were estimated to be in the region of 50−100 Å$^2$. Although these values do not correspond to different conformations, differences in cross-sectional area of this order can be envisaged for conformational changes. Indeed, for the MI-MII transition of rhodopsin, and for transitions between the conductance levels of alamethicin channels, conformational changes corresponding to changes in cross-sectional area of 80−110 Å$^2$ were estimated. For a protein of mean cross-sectional radius $r_P \approx 20$ Å, such as rhodopsin (79), a change in cross-sectional area by 100 Å$^2$ would correspond to a change in cross-sectional radius of $\Delta r_P \approx 1$ Å. A change of this magnitude would involve the displacement, or incorporation, of effectively just one lipid in the first shell at the perimeter of the transmembrane protein. Correspondingly, experiments with spin-labeled lipids do not detect a significant change in the number of first-shell lipids on mild bleaching of rhodopsin to the meta-II state (97).

Because rhodopsin displays little, or no, lipid headgroup selectivity (74,98,99), the influence of lipid-protein interactions should be felt primarily in the lipid chain regions. With a change in excess free energy density of $\Delta g_{LP}^{(ch)} \approx 60$ J mol$^{-1}$ per Å$^2$ (see above) and a hydrophobic span for rhodopsin of 32 ± 2 Å (100), Eq. 24 then predicts a maximum change in chemical potential on changing lipid chain composition of 12 ± 1 kJ mol$^{-1}$ for a conformational change with $\Delta r_P \approx 1$ Å. This would shift relative conformational equilibrium populations of the meta-I and meta-II states by 100-fold. Similar estimates based on the selectivity of lipid headgroup interactions with other integral proteins yield changes in chemical potential of the protein in the range of $+4$ to $-11$ kJ mol$^{-1}$, relative to phosphatidylcholine, for a protein of the same size as rhodopsin.

For estimation of the effect of changing lipid chain composition, it was tacitly assumed that the conformational change is referred to a hypothetical lipid environment for which $g_{LP}^{(ch)} = 0$. A vanishing excess free energy ($g_{LP} = 0$) implies simply that the lipid-protein interaction is isoenergetic with the lipid-lipid interactions that occur within the bulk bilayer regions of the membrane. The considerable reduction in $g_{LP}^{(ch)}$, relative to saturated lipids associated with rhodopsin, that is found for monounsaturated lipids interacting with the $Ca^{2+}$-ATPase suggests that such a situation (i.e., $g_{LP}^{(ch)} = 0$) is not unrealistic. An alternative situation is one in which the two conformations of the protein present different hydrophobic spans to the lipid. The reference state would then correspond to a lipid whose chainlength just matches that of the conformation with shorter hydrophobic span.

## Highly curved lipid vesicles

The formulation of the lipid-protein interaction in terms of bending energies (i.e., Eqs. 12 and 13) that was given above allows investigation of the effects of vesicle curvature, e.g., for small unilamellar vesicles (SUVs). When the reference state in the absence of protein is not a planar bilayer, the curvature energies of the outer and inner monolayers must be considered explicitly (see Fig. 7). The areas, $A_n$, at the neutral surfaces of the outer and inner monolayers in a curved bilayer are given by simple geometry,

$$A_n = A(1 \pm \delta c_1)(1 \pm \delta c_2) = A(1 \pm \delta\bar{c} + \delta^2\bar{c}_G^2), \quad (25)$$

where $A$, $\bar{c}$, and $\bar{c}_G$ are the area, the mean curvature, and the Gaussian curvature, respectively, at the bilayer midplane, and $\delta$ is the distance of the neutral surface from the midplane. The upper signs in Eq. 25 correspond to the neutral surface of the outer monolayer and the lower signs to that of the inner monolayer. The mean curvatures, $\bar{c}_n$, of the neutral surfaces are then given by

$$\bar{c}_n = \pm\left(\frac{1}{R_1 \pm \delta} + \frac{1}{R_2 \pm \delta}\right) = \pm\,(\bar{c} \pm 2\delta\bar{c}_G^2)\frac{A}{A_n} \quad (26)$$

and the Gaussian curvatures, $\bar{c}_{G,n}^2$, at the neutral surfaces are given similarly by

$$\bar{c}_{G,n}^2 = \frac{1}{(R_1 \pm \delta)(R_2 \pm \delta)} = \bar{c}_G^2\,\frac{A}{A_n}, \quad (27)$$

where the upper and lower signs refer to the outer and inner monolayers, respectively, as in the corresponding expressions for $A_n$.

Adding free energy contributions from the outer and inner monolayers of the bilayer membrane according to Eq. 12, and discarding terms of fourth order or higher in the membrane curvature, $\bar{c}$ and $\bar{c}_G$, gives the following expression for the total bending free energy,

$$\Delta G_c^{(b)}(\bar{c},\bar{c}_G) = k_c A(\bar{c}^2 + c_o^2) + 2(\bar{k}_c - 2k_c\delta c_o + k_c\delta^2 c_o^2/2)A\bar{c}_G^2, \quad (28)$$

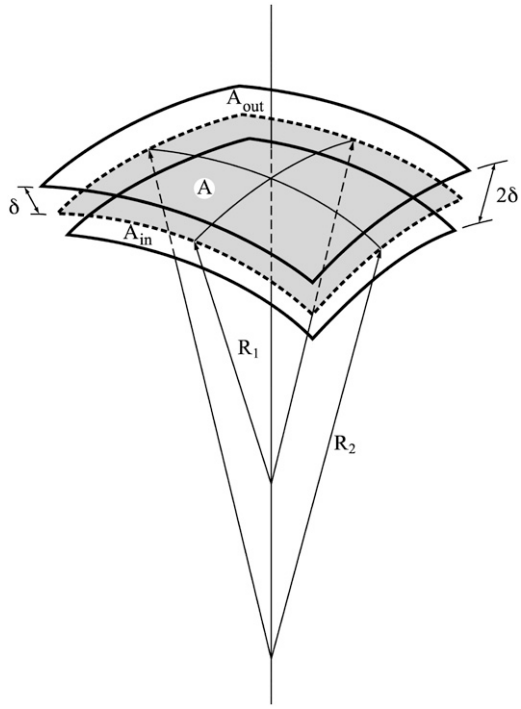


FIGURE 7 Geometry of outer (*out*) and inner (*in*) monolayers in a curved bilayer. Curvatures of the two neutral surfaces are given by $c_{1,2}^{\text{out}} = 1/(R_{1,2}+\delta)$ and $c_{1,2}^{\text{in}} = -1/(R_{1,2}-\delta)$, where $R_{1,2}$ are the principal radii of curvature of the bilayer midplane and $\delta$ is the distance of the neutral surface from the bilayer midplane. Areas at the two neutral surfaces are $A_{\text{out}} = A(1+\delta c_1)(1+\delta c_2)$ and $A_{\text{in}} = A(1-\delta c_1)(1-\delta c_2)$, where $A$ is the corresponding area at the bilayer midplane, and $c_1$ and $c_2$ are the principal curvatures of the midplane.

which involves no truncation for completely spherical deformations. Note that the constant term $k_c A c_o^2$ on the right of Eq. 28 represents curvature frustration of the individual monolayers and does not contribute to the energy of bending a symmetrical bilayer. For a spherical vesicle of radius $R$, the curvature free energy is given by Eq. 28 with $\bar{c}/2 = \bar{c}_G \equiv c = 1/R$. The chemical potential of a protein in this curved vesicle is then given by

$$\mu_b = \mu_b^o + k_B T \ln(X_b) + n_b A_L k_c[(\bar{c}_{G,P}^2 - c^2) \times (\delta^2 c_o^2 - 4\delta c_o + 2\bar{k}_c/k_c) + \bar{c}_P^2 - 4c^2], \qquad (29)$$

where $c$ and $A_L$ refer to the bilayer midplane (see Fig. 7). In the case of a curved vesicle, the contributions of the lateral pressure profile to the chemical potential of the inserted protein include a term that depends quadratically on the spontaneous curvature of the lipids, not simply the linear term plus a constant that is found for a planar bilayer (compare with Eq. 13). Assuming linear additivity of spontaneous curvatures according to Eq. 18, the ratio of the coefficients of the quadratic to the linear term in mole fraction, $X$, of component 2 in Eq. 29 should be $-(\delta/2)(c_{o,2} - c_{o,1})/(2 - \delta c_{o,1}) \approx -(\delta/4)(c_{o,2} - c_{o,1})$, because $c_{o,1} \ll 1/\delta$. Taking values appropriate to DOPE and DOPC gives a ratio of $\approx 0.1$, which means that the quadratic term is relatively insignificant in comparison with the term that is linear in $X$, even for $X = 1$.

## Folding of OmpA in SUVs

Hong and Tamm (26), in a series of experiments with systematically varying lipid composition, have demonstrated reversible urea-induced unfolding of the $\beta$-barrel outer membrane protein OmpA in small unilamellar vesicles (SUVs of mean diameter 300 Å). OmpA that has been unfolded in urea inserts and folds spontaneously into SUVs composed of phosphatidylcholines of normal chainlengths (101), but not into large unilamellar vesicles unless the chainlength of the constituent lipids is 12 C-atoms or less (102). Vesicle curvature therefore plays a very significant role in the energetics of folding of OmpA in membranes composed of lipids with chainlengths greater than 12 C-atoms. This should be taken into account explicitly in analysis of the effects of spontaneous lipid curvature on the stability of membrane-bound OmpA.

The free energy of unfolding of OmpA in SUVs composed of mixtures of POPC with POPE, taken from the work of Hong and Tamm (26), is shown in Fig. 8. From the linear regression data, the gradient $\partial\mu_b/\partial X$ with respect to mole fraction of POPE, which from Eqs. 18 and 29 should be equal to $-2n_L A_L k_c(\bar{c}_{G,P}^2 - c^2)\delta(c_o^{\text{POPE}} - c_o^{\text{POPC}})(2 - \delta c_o^{\text{POPC}})$, has a value of $\sim 23 \pm 5$ kJ mol$^{-1}$.

The number of first-shell lipids that can be accommodated around the intramembranous perimeter of OmpA is $n_L \approx 20 \pm 2$ (49). Unfortunately, values of the spontaneous curvature are not available for POPE and POPC, but taking the corresponding values for DOPE and DOPC (see Fig. 4) yields a value of $\bar{c}_{G,P} \approx \pm(0.021 \pm 0.006)$Å$^{-1}$. Examina-

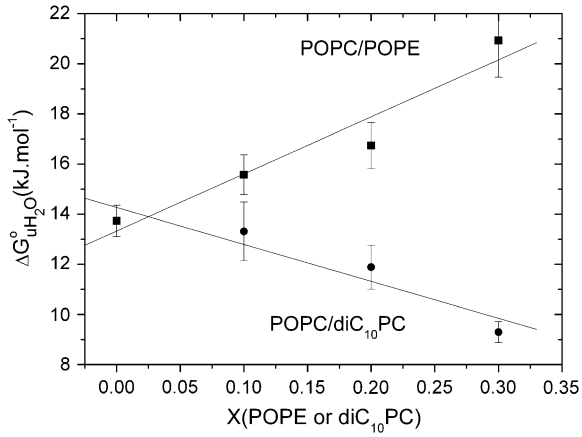


FIGURE 8 Dependence of the free energy of unfolding ($\Delta G_{u,H_2O}^o$) of OmpA on lipid composition in SUVs of POPC containing mole fraction, $X$, of either POPE (*squares*) or diC$_{10}$PC (*circles*). $T$ = 37.5°C. (Data from (26).) The solid lines are linear regressions.

tion of the intramembranous shape of OmpA reveals that this would favor lipids with negative curvature (26,103). In SUVs, the lipids of the outer monolayer assume a positive curvature, whereas those of the inner monolayer possess a rather strong negative curvature. The latter probably account for the ability of SUVs of POPC and DOPC to incorporate OmpA spontaneously. However, the situation may be complicated by an asymmetric distribution of lipids between the outer and inner monolayers, and by the possibility of lipid redistribution between the two monolayers on protein incorporation (104). Note that the contribution of vesicle curvature according to Eq. 29 scales as $(c/\bar{c}_{G,P})^2$, which is 10% in this particular case. Intrinsic lipid curvature is not the only factor stabilizing folded OmpA in SUVs relative to large unilamellar vesicles (104).

The free energy of unfolding of OmpA in SUVs of POPC mixed with didecanoyl phosphatidylcholine ($diC_{10}PC$) is also shown in Fig. 8. Admixture with this short-chain lipid progressively reduces the free energy of unfolding, in contrast to the situation with POPE. From the linear regression, the gradient of the free energy with respect to mole fraction of $diC_{10}PC$ is $\partial\mu_b/\partial X = -(15 \pm 3)$ kJ mol$^{-1}$. The spontaneous curvature of $diC_{10}PC$ is not known but, for such a short-chain lipid with large headgroup, it is expected to be positive (see Eq. 14 and Fig. 3). From the ratio of the gradient with respect to that for POPE in Fig. 8, it can be estimated that the spontaneous curvature of $diC_{10}PC$ is $c_o \sim +0.02 \pm 0.01$ Å$^{-1}$, again assuming the values of DOPC and DOPE for POPC and POPE, respectively. As in considerations of DMPC interacting with CCT (see above), this is a lower estimate for the spontaneous curvature of $diC_{10}PC$ because it ignores differences in bending rigidity. The opposite sign of $c_o$ for $diC_{10}PC$ relative to POPE is again a strong indicator of the importance of lipid curvature in insertion and folding of OmpA.

That the intramembrane shape of OmpA favors lipids with negative spontaneous curvature can be attributed, at least in part, to the two belts of aromatic side chains (especially tryptophan) that are located at the polar-apolar interfaces of the membrane (105). This feature is common not only to $\beta$-barrel outer membrane proteins, but also to most $\alpha$-helical transmembrane proteins, with the notable exception of rhodopsin. A further contributing factor is the shape of the polypeptide backbone of the barrel, which is determined by the twist, $\theta$, of the $\beta$-sheets and the coiling angle, $\varepsilon$, of their strands. Murzin et al. (106) have shown by using differential geometry that the transmembrane profile of the $\beta$-barrel radius, $R(z)$, is given by

$$R(z) - R(0) = \left[\frac{h}{d}\theta\sin 2\beta - \varepsilon\cos^2\beta - \frac{h}{d}\eta\sin^2\beta\right] z^2/2h, \tag{30}$$

where $\eta$ is the coiling angle perpendicular to the strand, $\beta$ is the tilt of the strands within the sheet, $h$ is the rise per residue along the strand, and $d$ is the separation between adjacent strands. Using parameters for the strand geometry appropriate to a $\beta$-barrel such as OmpA, which has $n = 8$ strands and a shear number of $S = 10$ (107,108), Eq. 30 predicts that the barrel radius at the neutral planes is $R(\pm\delta) = 9.5$ Å, in comparison with $R(0) = 8.2$ Å at the membrane midplane. Thus, the shape of the barrel backbone corresponds to a hyperboloid of revolution and the increased cross-sectional area at the neutral surfaces favors lipids with negative intrinsic curvature.

## Refolding of bacteriorhodopsin

Allen et al. (109) have investigated the refolding of an $\alpha$-helical transmembrane protein, bacteriorhodopsin (bR), that was denatured in sodium dodecylsulphate. This was done by diluting into a dispersion of 500 Å-diameter lipid vesicles composed of dipalmitoleoyl phosphatidylcholine ($diC_{16:1}PC$) with varying proportions of lipids that have different spontaneous curvatures. Fig. 9 shows the fractional folding-yield, $f$, as a function of the mole fraction of dipalmitoleoyl phosphatidylethanolamine ($diC_{16:1}PE$), DMPC, or lyso palmitoyl phosphatidylcholine (lysoPPC) in the phospholipid mixture. In addition, the vesicles contained an estimated 20 mol % of residual sodium dodecylsulphate. Unlike the situation with the $\beta$-barrel protein OmpA, the folding of the seven-helix bundle of bR is disfavored by admixture of the $diC_{16:1}PE$, which has more negative spontaneous curvature than $diC_{16:1}PC$.

Whereas the experimental protocol employed for refolding may not strictly allow application of equilibrium thermodynamics, it is of interest to pursue this avenue for comparative purposes. In Fig. 9, the folding yield is expressed in terms of an effective equilibrium constant: $K = f/(1-f)$ and thus the ordinate is effectively a free energy of unfolding.

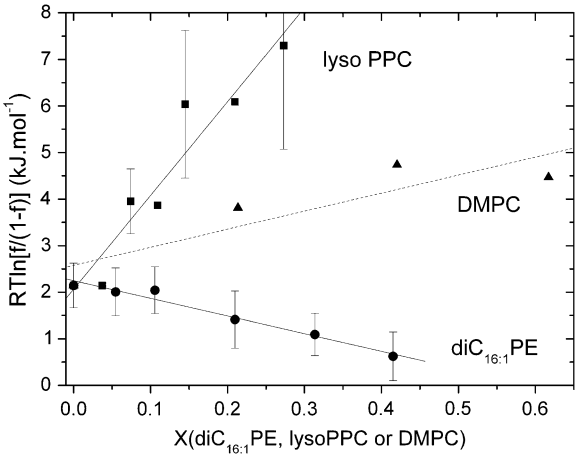


FIGURE 9 Dependence of the fractional refolding, $f$, of bacteriorhodopsin in 500 Å-diameter vesicles of $diC_{16:1}PC$ on mole fraction, $X$, of additional $diC_{16:1}PE$ (*circles*), lysoPPC (*squares*), or DMPC (*triangles*). $T = 25$°C. (Data from (109)). Fractional refolding is expressed as the ratio $f/(1-f)$ of folded to unfolded species, and hence the ordinate (where $R$ is the ideal gas constant and $T$ is the absolute temperature) is an effective unfolding free energy.

The dependence on mol fraction of $diC_{16:1}PE$ in the vesicles is linear and deductions from the slope in Fig. 9 by using Eq. 29, as was done in the case of OmpA, yields an effective curvature of the protein-associated lipids of $\bar{c}_{G,P} = \pm (0.008 \pm 0.001)$Å$^{-1}$. For this estimate $n_L = 25 \pm 2$ was assumed for bR (49) and again the spontaneous curvatures of DOPC and DOPE were taken as representative of $diC_{16:1}PC$ and $diC_{16:1}PE$, respectively. Clearly, the positive sign (i.e., that opposite to OmpA) is appropriate for the spontaneous curvature associated with bR. Despite approximations and uncertainties, the absolute magnitude of the spontaneous curvature is rather small for a membrane insertion process, as might be anticipated because the helices of bR are relatively straight and untilted compared with those of rhodopsin (110,111). In consequence, the intramembrane cross-sectional dimensions (~38 Å × 23 Å; (112)) are less than those of rhodopsin, corresponding to a cross-sectional area of $A_P \sim 690$ Å$^2$ (see also (113)). For these reasons, the absolute value of the effective lipid curvature on folding and membrane insertion of bR is similar to that for a conformational change (MI to MII) in membrane-bound rhodopsin.

Fig. 9 shows that lysoPPC, which is expected to have a spontaneous curvature opposite to that of $diC_{16:1}PE$, enhances the folding yield relative to $diC_{16:1}PC$. To a lesser extent, so does DMPC. From the ratio of gradients in Fig. 9 it can be deduced that the spontaneous curvatures $\Delta c_o$ of lysoPPC and $diC_{16:1}PE$, referred to that of $diC_{16:1}PC$, are in the ratio $-5.3 \pm 1.2$, and for DMPC the ratio is $-1.0 \pm 0.5$. Based on molecular shapes, the spontaneous curvature of lysoPPC is undoubtedly opposite in sign to that of $diC_{16:1}PE$, and therefore the opposite effects on folding yield indicate a mechanism involving intrinsic lipid curvature.

## CONCLUSIONS

Table 1 summarizes results from analyses of the dependence of protein (or peptide) insertion or activity on the intrinsic curvature, $c_o$, of the host membrane lipids. Characterization is given in terms both of the cross-sectional shape, $A_P(\delta)-A_P(0)$ (i.e., the transverse area of the protein at the monolayer neutral plane, relative to that at the membrane midplane), and of the effective curvature, $\bar{c}_P$, of lipids situated at the intramembranous perimeter of the protein. These are based on Eqs. 11 and 13, respectively, where values of $a_{1,P}\delta + 2a_{2,P}\delta^2$ obtained for the former are an upper estimate for $A_P(\delta)-A_P(0) = a_{1,P}\delta + a_{2,P}\delta^2$.

Results for alamethicin, CCT, rhodopsin, and bacteriorhodopsin are likely to be more representative of those for typical $\alpha$-helical transmembrane proteins than are those for MscL. The large cross-sectional changes that take place with the latter are almost certainly a special feature of channels that are sensitive to membrane stretch. The value of $\bar{c}_P$ estimated for the small $\beta$-barrel protein OmpA is greater than that for the alamethicin monomer, but less than that found for CCT. Data for the isolated alamethicin monomer and for CCT correspond to insertion of the protein in the membrane, as do those for the refolding of OmpA and bacteriorhodopsin. These therefore refer to the absolute values of $A_P(\delta)$-$A_P(0)$ and of $\bar{c}_P$ for the membrane-penetrant section of the protein. Data for rhodopsin, MscL, KvAP, and alamethicin channels, on the other hand, correspond to functional changes in conformation of the membrane-bound protein. These therefore refer to differences in $A_P(\delta)-A_P(0)$ and $\bar{c}_P$ between the two conformational states, e.g., MI and MII, or open and closed. Some conformational changes of transmembrane proteins, however, may not involve appreciable changes in intramembrane shape. For instance, the $K_d$ for $Ca^{2+}$-binding to the SERCA Ca-ATPase, which is thought to be related to the E1/E2 state conformational equilibrium, remains unchanged on replacing DOPC by a 4:1 DOPE:DOPC mixture (114).

Not all responses of transmembrane proteins to phospholipid composition are necessarily attributable to spontaneous curvature frustration of the membrane lipids (see, e.g., (115)). Prominent among these is, for instance, hydrophobic matching (89,116,117). In this respect, two features can be considered as diagnostic for lipid curvature contributions. One feature is the systematic response to DOPC-DOPE mixtures, because these two lipids differ markedly in their spontaneous curvature (see Fig. 4), whereas diffraction results show their lipid thicknesses in $H_{II}$-phases to be practically identical (16). Much of the analysis given here is based on mixtures of these two lipids (or of the analogous POPC-POPE mixtures). The second feature is the opposite response induced by lipids of opposite spontaneous curvatures. This is in contrast to the

**TABLE 1 Changes in cross-sectional shape, $A_P(\delta)-A_P(0)$, or in curvature, $\bar{c}_P$, of associated lipids, on conformational changes, folding or insertion of peptides, or proteins in membranes**

| Protein/peptide* | $A_P(\delta)$-$A_P(0)$ (Å$^2$) | $\bar{c}_P$ (Å$^{-1}$) |
|---|---|---|
| Alm monomer | | |
| Isolated[†] | −100 ± 20 | +0.011 ± 0.004 |
| in channel[‡] | +80 ± 20 | +0.007 ± 0.006 |
| CCT[†] | +47 ± 16 | −0.0035 ± 0.0015 |
| Rho[§] | +112 ± 25 | −0.006 ± 0.002 |
| MscL[§] | −595 ± 90 | +0.024 ± 0.004 |
| KvAP[§] | 150 ± 30 | |
| OmpA[†¶] | | −0.021 ± 0.006[‖] |
| bR[†¶] | | +0.008 ± 0.001[‖] |

Deduced from dependence on spontaneous curvature of host lipids. $A_P(\delta)-A_P(0)$ is the difference in transverse cross-sectional area of the protein between the membrane midplane and the neutral plane of one bilayer half. The values given, viz., $a_{1,P}\delta + 2a_{2,P}\delta^2$, are an upper estimate for this quantity.

*Alm, alamethicin (21,22); CCT, CTP:phosphocholine cytidylyltransferase (24); Rho, bovine rhodopsin (25); MscL, mechanosensitive channel of large conductance (81); KvAP, voltage-dependent $K^+$-channel (86); OmpA, *Escherichia coli* outer membrane protein A (26); bR, bacteriorhodopsin (109).

[†]Insertion.

[‡]Oligomerization.

[§]Conformational change.

[¶]Folding.

[‖]$\bar{c}_{G,P}$, although $\bar{c}_P$ derived assuming a planar membrane is of a similar magnitude.

effect of lipids that are too long or too short to achieve hydrophobic matching, the effects of which are in the same direction. In the examples considered here, the opposite effect to that of the negative-curvature lipid PE is afforded by lyso or short-chain saturated PCs, which have positive spontaneous curvature.

Finally, from the point of view of functional protein control, it should be pointed out that spontaneous curvature can be modulated not only by varying lipid composition but also by changing pH or ionic conditions (118,119), or by protein binding (120) or enzymatic lipid hydrolysis (121,122), or even by varying protein concentration (123). In this way, function may be triggered by means that potentially are more rapid than metabolic control of lipid composition.

I thank the anonymous reviewers of this article for their most helpful and informative comments.

## REFERENCES


1. Marsh, D. 1996. Lateral pressure in membranes. *Biochim. Biophys. Acta.* 1286:183–223.
2. Bezrukov, S. M. 2000. Functional consequences of lipid packing stress. *Curr. Opin. Colloid Interface Sci.* 5:237–243.
3. Brink-van der Laan, E. V., J. A. Killian, and B. De Kruijff. 2004. Nonbilayer lipids affect peripheral and integral membrane proteins via changes in the lateral pressure profile. *Biochim. Biophys. Acta.* 1666: 275–288.
4. Evans, E. A., and R. Waugh. 1977. Mechano-chemistry of closed, vesicular membrane systems. *J. Colloid Interface Sci.* 60:286–298.
5. Lindahl, E., and O. Edholm. 2000. Spatial and energetic entropic decomposition of surface tension in lipid bilayers from molecular dynamics simulations. *J. Chem. Phys.* 113:3882–3893.
6. Gullingsrud, J., and K. Schulten. 2004. Lipid bilayer pressure profiles and mechanosensitive channel gating. *Biophys. J.* 86:3496–3509.
7. Marsh, D. 2006. Comment on interpretation of mechanochemical properties of lipid bilayer vesicles from the equation of state or pressure-area measurement of the monolayer at the air-water or oil-water interface. *Langmuir.* 22:2916–2919.
8. Cevc, G., and D. Marsh. 1987. Phospholipid Bilayers. Physical Principles and Models. Wiley-Interscience, New York.
9. Cantor, R. S. 1997. Lateral pressures in cell membranes: a mechanism for modulation of protein function. *J. Phys. Chem. B.* 101:1723–1725.
10. Cantor, R. S. 1999. The influence of membrane lateral pressures on simple geometric models of protein conformational equilibria. *Chem. Phys. Lipids.* 101:45–56.
11. Cantor, R. S. 2002. Size distribution of barrel-stave aggregates of membrane peptides: influence of the bilayer lateral pressure profile. *Biophys. J.* 82:2520–2525.
12. Cantor, R. S. 1999. Lipid composition and the lateral pressure profile in bilayers. *Biophys. J.* 76:2625–2639.
13. Lee, A. G. 2004. How lipids affect the activities of integral membrane proteins. *Biochim. Biophys. Acta.* 1666:62–87.
14. Helfrich, W. 1981. Amphiphilic mesophases made of defects. *In* Physics of Defects. R. Balian, M. Kléman, and J. P. Poirier, editors. North-Holland Publishing, Amsterdam. 716–755.
15. Marsh, D. 2001. Elastic constants of polymer-grafted lipid membranes. *Biophys. J.* 81:2154–2162.
16. Rand, R. P., N. L. Fuller, S. Gruner, and V. A. Parsegian. 1990. Membrane curvature, lipid segregation, and structural transitions for phospholipids under dual-solvent stress. *Biochemistry.* 29:76–87.
17. Leikin, S., M. M. Kozlov, N. L. Fuller, and R. P. Rand. 1996. Measured effects of diacylglycerol on structural and elastic properties of phospholipid membranes. *Biophys. J.* 71:2623–2632.
18. Chen, Z., and R. P. Rand. 1997. The influence of cholesterol on phospholipid membrane curvature and bending elasticity. *Biophys. J.* 73:267–276.
19. Fuller, N., and R. P. Rand. 2001. The influence of lysolipids on the spontaneous curvature and bending elasticity of phospholipid membranes. *Biophys. J.* 81:243–254.
20. Fuller, N., C. R. Benatti, and R. P. Rand. 2003. Curvature and bending constants for phosphatidylserine-containing membranes. *Biophys. J.* 85:1667–1674.
21. Keller, S. L., S. M. Bezrukov, S. M. Gruner, M. W. Tate, I. Vodyanoy, and V. A. Parsegian. 1993. Probability of alamethicin conductance states varies with nonlamellar tendency of bilayer phospholipids. *Biophys. J.* 65:23–27.
22. Lewis, J. R., and D. S. Cafiso. 1999. Correlation between the free energy of a channel-forming voltage-gated peptide and the spontaneous curvature of bilayer lipids. *Biochemistry.* 38:5932–5938.
23. Curran, A. R., R. H. Templer, and P. J. Booth. 1999. Modulation of folding and assembly of the membrane protein bacteriorhodopsin by intermolecular forces within the lipid bilayer. *Biochemistry.* 38:9328–9336.
24. Attard, G. S., R. H. Templer, W. S. Smith, A. N. Hunt, and S. Jackowski. 2000. Modulation of CTP:phosphocholine cytidylyltransferase by membrane curvature elastic stress. *Proc. Natl. Acad. Sci. USA.* 97:9032–9036.
25. Botelho, A. V., N. J. Gibson, R. L. Thurmond, Y. Wang, and M. F. Brown. 2002. Conformational energetics of rhodopsin modulated by nonlamellar-forming lipids. *Biochemistry.* 41:6354–6368.
26. Hong, H., and L. K. Tamm. 2004. Elastic coupling of integral membrane protein stability to lipid bilayer forces. *Proc. Natl. Acad. Sci. USA.* 101:4065–4070.
27. Helfrich, W. 1973. Elastic properties of lipid bilayers: theory and possible experiments. *Z. Naturforsch.* 28c:693–703.
28. Gruner, S. M. 1985. Intrinsic curvature hypothesis for biomembrane lipid composition: a role for non-bilayer lipids. *Proc. Natl. Acad. Sci. USA.* 82:3665–3669.
29. Seddon, J. M. 1990. Structure of the inverted hexagonal ($H_{II}$) phase, and non-lamellar phase transitions of lipids. *Biochim. Biophys. Acta.* 1031:1–69.
30. Seddon, J. M., and R. H. Templer. 1995. Polymorphism and lipid-water systems. *In* Structure and Dynamics of Membranes. R. Lipowsky and E. Sackmann, editors. Elsevier SPC, Amsterdam. 97–160.
31. Marsh, D. 2001. Polarity and permeation profiles in lipid membranes. *Proc. Natl. Acad. Sci. USA.* 98:7777–7782.
32. Marsh, D. 2002. Membrane water-penetration profiles from spin labels. *Eur. Biophys. J.* 31:559–562.
33. Kurad, D., G. Jeschke, and D. Marsh. 2003. Lipid membrane polarity profiles by high-field EPR. *Biophys. J.* 85:1025–1033.
34. Bartucci, R., R. Guzzi, D. Marsh, and L. Sportelli. 2003. Intramembrane polarity by electron spin echo spectroscopy of labeled lipids. *Biophys. J.* 84:1025–1030.
35. Bartucci, R., D. A. Erilov, R. Guzzi, L. Sportelli, S. A. Dzuba, and D. Marsh. 2006. Time-resolved electron spin resonance studies of spin-labeled lipids in membranes. *Chem. Phys. Lipids.* 141:142–157.
36. Erilov, D. A., R. Bartucci, R. Guzzi, A. A. Shubin, A. G. Maryasov, D. Marsh, S. A. Dzuba, and L. Sportelli. 2005. Water concentration profiles in membranes measured by ESEEM of spin-labeled lipids. *J. Phys. Chem. B.* 109:12003–12013.
37. King, M. D., and D. Marsh. 1987. Headgroup and chain length dependence of phospholipid self-assembly studied by spin-label electron spin resonance. *Biochemistry.* 26:1224–1231.
38. Aveyard, R., and D. A. Haydon. 1965. Thermodynamic properties of aliphatic hydrocarbon/water interfaces. *J. Colloid Interface Sci.* 20: 2255–2261.

39. Marsh, D. 1996. Components of the lateral pressure in lipid bilayers deduced from $H_{II}$ phase dimensions. *Biochim. Biophys. Acta.* 1279: 119–123.
40. Szleifer, I., D. Kramer, A. Ben-Shaul, W. M. Gelbart, and S. A. Safran. 1990. Molecular theory of curvature elasticity in surfactant films. *J. Chem. Phys.* 92:6800–6817.
41. Milner, S. T., and T. A. Witten. 1988. Bending moduli of polymeric surfactant interfaces. *J. de Phys.* 49:1951–1962.
42. Rawicz, W., K. C. Olbrich, T. McIntosh, D. Needham, and E. Evans. 2000. Effect of chain length and unsaturation on elasticity of lipid bilayers. *Biophys. J.* 79:328–339.
43. Templer, R. H., B. J. Khoo, and J. M. Seddon. 1998. Gaussian curvature modulus of an amphiphilic monolayer. *Langmuir.* 14:7427–7434.
44. Siegel, D. P., and M. M. Kozlov. 2004. The Gaussian curvature elastic modulus of *N*-monomethylated dioleoylphosphatidylethanolamine: relevance to membrane fusion and lipid phase behavior. *Biophys. J.* 87:366–374.
45. Liu, Y. F., and J. F. Nagle. 2004. Diffuse scattering provides material parameters and electron density profiles of biomembranes. *Phys. Rev. E.* 69:040901.
46. Nielsen, C., M. Goulian, and O. S. Andersen. 1998. Energetics of inclusion-induced bilayer deformations. *Biophys. J.* 74:1966–1983.
47. Harroun, T. A., W. T. Heller, T. M. Weiss, L. Yang, and H. W. Huang. 1999. Theoretical analysis of hydrophobic matching and membrane-mediated interactions in lipid bilayers containing gramicidin. *Biophys. J.* 76:3176–3185.
48. Marsh, D. 1997. Stoichiometry of lipid-protein interaction and integral membrane protein structure. *Eur. Biophys. J.* 26:203–208.
49. Páli, T., D. Bashtovyy, and D. Marsh. 2006. Stoichiometry of lipid interaction with transmembrane proteins, deduced from the 3-D structures. *Protein Sci.* 15:1153–1161.
50. Marsh, D., A. Watts, W. Maschke, and P. F. Knowles. 1978. Protein-immobilized lipid in dimyristoylphosphatidylcholine-substituted cytochrome oxidase: evidence for both boundary and trapped-bilayer lipid. *Biochem. Biophys. Res. Commun.* 81:403–409.
51. Knowles, P. F., A. Watts, and D. Marsh. 1979. Spin label studies of lipid immobilization in dimyristoylphosphatidylcholine-substituted cytochrome oxidase. *Biochemistry.* 18:4480–4487.
52. Marsh, D. 1996. Intrinsic curvature in normal and inverted lipid structures and in membranes. *Biophys. J.* 70:2248–2255.
53. Marsh, D. 1997. Nonlamellar packing parameters for diacylglycerols. *Biophys. J.* 72:2834–2836.
54. Sen, A., T. V. Isac, and S.-W. Hui. 1991. Bilayer packing stress and defects in mixed dilinoleoylphosphatidylethanolamine and palmitoyloleoylphosphatidylcholine and their susceptibility to phospholipase $A_2$. *Biochemistry.* 30:4516–4521.
55. Helfrich, W. 1974. Blocked lipid exchange in bilayers and its possible influence on the shape of vesicles. *Z. Naturforsch.* 29c:510–515.
56. Southwell, R. V. 1941. An Introduction to the Theory of Elasticity. Oxford University Press, London.
57. Lorenzen, S., R. M. Servuss, and W. Helfrich. 1986. Elastic torques about membrane edges—a study of pierced egg lecithin vesicles. *Biophys. J.* 50:565–572.
58. Marsh, D. 2006. Elastic curvature constants of lipid monolayers and bilayers. *Chem. Phys. Lipids.* 144:146–159.
59. Marsh, D., and L. I. Horváth. 1998. Structure, dynamics and composition of the lipid-protein interface. Perspectives from spin-labeling. *Biochim. Biophys. Acta.* 1376:267–296.
60. Fretten, P., S. J. Morris, A. Watts, and D. Marsh. 1980. Lipid-lipid and lipid-protein interactions in chromaffin granule membranes. *Biochim. Biophys. Acta.* 598:247–259.
61. Pates, R. D., and D. Marsh. 1987. Lipid mobility and order in bovine rod outer segment disk membranes. A spin-label study of lipid-protein interactions. *Biochemistry.* 26:29–39.
62. Esmann, M., A. Watts, and D. Marsh. 1985. Spin-label studies of lipid-protein interactions in $(Na^+,K^+)$-ATPase membranes from rectal glands of *Squalus acanthias*. *Biochemistry.* 24:1386–1393.
63. Marsh, D., A. Watts, and F. J. Barrantes. 1981. Phospholipid chain immobilization and steroid rotational immobilization in acetylcholine receptor-rich membranes from *Torpedo marmorata*. *Biochim. Biophys. Acta.* 645:97–101.
64. Horváth, L. I., P. J. Brophy, and D. Marsh. 1988. Influence of lipid headgroup on the specificity and exchange dynamics in lipid-protein interactions. A spin label study of myelin proteolipid apoprotein-phospholipid complexes. *Biochemistry.* 27:5296–5304.
65. Barranger-Mathys, M., and D. S. Cafiso. 1994. Collisions between helical peptides in membranes monitored using electron paramagnetic resonance: evidence that alamethicin is monomeric in the absence of a membrane potential. *Biophys. J.* 67:172–176.
66. Marsh, D., M. Jost, C. Peggion, and C. Toniolo. 2007. TOAC spin labels in the backbone of alamethicin: EPR studies in lipid membranes. *Biophys. J.* 92:473–481.
67. Marsh, D., M. Jost, C. Peggion, and C. Toniolo. 2007. Lipid chainlength dependence for incorporation of alamethicin in membranes: EPR studies on TOAC-spin labeled analogues. *Biophys. J.* 92: 4002–4011.
68. Fox, R. O., Jr., and F. M. Richards. 1982. A voltage-gated ion channel model inferred from the crystal structure of alamethicin at 1.5 Å resolution. *Nature.* 300:325–330.
69. Dan, N., and S. A. Safran. 1998. Effect of lipid characteristics on the structure of transmembrane proteins. *Biophys. J.* 75:1410–1414.
70. Marsh, D. 1999. Spin label ESR spectroscopy and FTIR spectroscopy for structural/dynamic measurements on ion channels. *Methods Enzymol.* 294:59–92.
71. Gruner, S. M., M. W. Tate, G. L. Kirk, P. T. C. So, D. C. Turner, D. T. Keane, C. P. S. Tilcock, and P. R. Cullis. 1988. X-ray diffraction study of the polymorphic behavior of *N*-methylated dioleoyl phosphatidylethanolamine. *Biochemistry.* 27:2853–2866.
72. Davies, S. M. A., R. M. Epand, R. Kraayenhof, and R. B. Cornell. 2001. Regulation of CTP: Phosphocholine cytidylyltransferase activity by the physical properties of lipid membranes: an important role for stored curvature strain energy. *Biochemistry.* 40:10522–10531.
73. Nagle, J. F., and S. Tristram-Nagle. 2000. Structure of lipid bilayers. *Biochim. Biophys. Acta.* 1469:159–195.
74. Watts, A., I. D. Volotovski, and D. Marsh. 1979. Rhodopsin-lipid associations in bovine rod outer segment membranes. Identification of immobilized lipid by spin labels. *Biochemistry.* 18:5006–5013.
75. Ryba, N. J. P., L. I. Horváth, A. Watts, and D. Marsh. 1987. Molecular exchange at the lipid-rhodopsin interface: spin-label electron spin resonance studies of rhodopsin-dimyristoyl phosphatidylcholine recombinants. *Biochemistry.* 26:3234–3240.
76. Ryba, N. J. P., and D. Marsh. 1992. Protein rotational diffusion and lipid/protein interactions in recombinants of bovine rhodopsin with saturated diacylphosphatidylcholines of different chain lengths studied by conventional and saturation transfer electron spin resonance. *Biochemistry.* 31:7511–7518.
77. Stenkamp, R. E., S. Filipek, C. A. G. G. Driessen, D. C. Teller, and K. Palczewski. 2002. Crystal structure of rhodopsin: a template for cone visual pigments and other G protein-coupled receptors. *Biochim. Biophys. Acta.* 1565:168–182.
78. Attwood, P. V., and H. Gutfreund. 1980. The application of pressure relaxation to the study of the equilibrium between metarhodopsin I and II from bovine retinas. *FEBS Lett.* 119:323–326.
79. Teller, D. C., T. Okada, C. A. Behnke, K. Palczewski, and R. E. Stenkamp. 2001. Advances in determination of a high-resolution three-dimensional structure of rhodopsin, a model of G-protein-coupled receptors (GPCRs). *Biochemistry.* 40:7761–7772.
80. Sukharev, S. I., W. J. Sigurdson, C. Kung, and F. Sachs. 1999. Energetic and spatial parameters for gating of the bacterial large conductance mechanosensitive channel, MscL. *J. Gen. Physiol.* 113:525–539.

81. Moe, P., and P. Blount. 2005. Assessment of potential stimuli for mechano-dependent gating of MscL: effects of pressure, tension, and lipid headgroups. *Biochemistry*. 44:12239–12244.
82. Chang, G., R. H. Spencer, A. T. Lee, M. T. Barclay, and D. C. Rees. 1998. Structure of the MscL homolog from *Mycobacterium tuberculosis*: a gated mechanosensitive ion channel. *Science*. 282:2220–2226.
83. Martinac, B., J. Adler, and C. Kung. 1990. Mechanosensitive ion channels of *E. coli* activated by amphipaths. *Nature*. 348:261–263.
84. Perozo, E., A. Kloda, D. M. Cortes, and B. Martinac. 2002. Physical principles underlying the transduction of bilayer deformation forces during mechanosensitive channel gating. *Nat. Struct. Biol*. 9:696–703.
85. Maingret, F., A. J. Patel, F. Lesage, M. Lazdunski, and E. Honore. 2000. Lysophospholipids open the two-pore domain mechano-gated $K^+$ channels TREK-1 and TRAAK. *J. Biol. Chem*. 275:10128–10133.
86. Schmidt, D., Q. X. Jiang, and R. MacKinnon. 2006. Phospholipids and the origin of cationic gating charges in voltage sensors. *Nature*. 444:775–779.
87. Marsh, D. 1995. Specificity of lipid-protein interactions. *In* Biomembranes. A. G. Lee, editor. JAI Press, Greenwich, CT. 137–186.
88. London, E., and G. W. Feigenson. 1981. Fluorescence quenching in model membranes. 2. Determination of the local lipid environment of the calcium adenosine triphosphatase from sarcoplasmic reticulum. *Biochemistry*. 20:1939–1948.
89. Lee, A. G. 2003. Lipid-protein interactions in biological membranes: a structural perspective. *Biochim. Biophys. Acta*. 1612:1–40.
90. Baldwin, P. A., and W. L. Hubbell. 1985. Effects of lipid environment on the light-induced conformational changes of rhodopsin. 2. Roles of lipid chain length, unsaturation, and phase state. *Biochemistry*. 24:2633–2639.
91. Caffrey, M., and G. W. Feigenson. 1981. Fluorescence quenching in model membranes. 3. Relationship between calcium adenosinetriphosphatase enzyme activity and the affinity of the protein for phosphatidylcholines with different acyl chain characteristics. *Biochemistry*. 20:1949–1961.
92. Small, D. M. 1986. The Physical Chemistry of Lipids. From Alkanes to Phospholipids. Plenum Press, New York and London.
93. Knowles, P. F., A. Watts, and D. Marsh. 1981. Spin label studies of headgroup specificity in the interaction of phospholipids with yeast cytochrome oxidase. *Biochemistry*. 20:5888–5894.
94. Esmann, M., and D. Marsh. 1985. Spin-label studies on the origin of the specificity of lipid-protein interactions in $Na^+$,$K^+$-ATPase membranes from *Squalus acanthias*. *Biochemistry*. 24:3572–3578.
95. Horváth, L. I., P. J. Brophy, and D. Marsh. 1990. Influence of polar residue deletions on lipid-protein interactions with the myelin proteolipid protein. Spin-label ESR studies with DM-20/lipid recombinants. *Biochemistry*. 29:2635–2638.
96. Pascher, I., M. Lundmark, P.-G. Nyholm, and S. Sundell. 1992. Crystal structures of membrane lipids. *Biochim. Biophys. Acta*. 1113:339–373.
97. Watts, A., J. Davoust, D. Marsh, and P. F. Devaux. 1981. Distinct states of lipid mobility in bovine rod outer segment membranes. Resolution of spin label results. *Biochim. Biophys. Acta*. 643:673–676.
98. Marsh, D., A. Watts, R. D. Pates, R. Uhl, P. F. Knowles, and M. Esmann. 1982. ESR spin label studies of lipid-protein interactions in membranes. *Biophys. J*. 37:265–274.
99. Pates, R. D., A. Watts, R. Uhl, and D. Marsh. 1985. Lipid-protein interactions in frog rod outer segment disc membranes. Characterization by spin labels. *Biochim. Biophys. Acta*. 814:389–397.
100. Lomize, M. A., A. L. Lomize, I. Pogozheva, and H. I. Mosberg. 2006. OPM: orientations of proteins in membranes database. *Bioinformatics*. 22:623–625.
101. Surrey, T., and F. Jähnig. 1992. Refolding and oriented insertion of a membrane protein into a lipid bilayer. *Proc. Natl. Acad. Sci. USA*. 89:7457–7461.
102. Kleinschmidt, J. H., and L. K. Tamm. 2002. Secondary and tertiary structure formation of the $\beta$-barrel membrane protein OmpA is synchronized and depends on membrane thickness. *J. Mol. Biol*. 324:319–330.
103. Marsh, D., B. Shanmugavadivu, and J. H. Kleinschmidt. 2006. Membrane elastic fluctuations and the insertion and tilt of $\beta$-barrel proteins. *Biophys. J*. 91:227–232.
104. Pocanschi, C. L., G. J. Patel, D. Marsh, and J. H. Kleinschmidt. 2006. Curvature elasticity and refolding of OmpA in large unilamellar vesicles. *Biophys. J*. 91:L75–L77.
105. Schulz, G. E. 2002. The structure of bacterial outer membrane proteins. *Biochim. Biophys. Acta*. 1565:308–317.
106. Murzin, A. G., A. M. Lesk, and C. Chothia. 1994. Principles determining the structure of $\beta$-sheet barrels in proteins. I. A theoretical analysis. *J. Mol. Biol*. 236:1369–1381.
107. Marsh, D. 2000. Infrared dichroism of twisted $\beta$-sheet barrels. The structure of *E. coli* outer membrane proteins. *J. Mol. Biol*. 297:803–808.
108. Páli, T., and D. Marsh. 2001. Tilt, twist and coiling in $\beta$-barrel membrane proteins: relation to infrared dichroism. *Biophys. J*. 80:2789–2797.
109. Allen, S. J., A. R. Curran, R. H. Templer, W. Meijberg, and P. J. Booth. 2004. Controlling the folding efficiency of an integral membrane protein. *J. Mol. Biol*. 342:1293–1304.
110. Luecke, H., B. Schobert, H.-T. Richter, J.-P. Cartailler, and J. K. Lanyi. 1999. Structure of bacteriorhodopsin at 1.55 Å resolution. *J. Mol. Biol*. 291:899–911.
111. Marsh, D., and T. Páli. 2001. Infrared dichroism from the x-ray structure of bacteriorhodopsin. *Biophys. J*. 80:305–312.
112. Henderson, R., J. M. Baldwin, T. A. Ceska, F. Zemlin, E. Beckmann, and K. H. Downing. 1990. Model for the structure of bacteriorhodopsin based on high-resolution electron cryomicroscopy. *J. Mol. Biol*. 213:899–929.
113. Glaeser, R. M., J. S. Jubb, and R. Henderson. 1985. Structural comparison of native and deoxycholate-treated purple membrane. *Biophys. J*. 48:775–780.
114. Starling, A. P., K. A. Dalton, J. M. East, S. Oliver, and A. G. Lee. 1996. Effects of phosphatidylethanolamines on the activity of the $Ca^{2+}$-ATPase of sarcoplasmic reticulum. *Biochem. J*. 320:309–314.
115. Lundbaek, J. A., P. Birn, A. J. Hansen, R. Sogaard, C. Nielsen, J. Girshman, M. J. Bruno, S. E. Tape, J. Egebjerg, D. V. Greathouse, G. L. Mattice, R. E. Koeppe, and O. S. Andersen. 2004. Regulation of sodium channel function by bilayer elasticity: the importance of hydrophobic coupling. Effects of micelle-forming amphiphiles and cholesterol. *J. Gen. Physiol*. 123:599–621.
116. Sperotto, M. M., and O. Mouritsen. 1991. Monte Carlo simulation studies of lipid order parameter profiles near integral membrane proteins. *Biophys. J*. 59:261–270.
117. de Planque, M. R. R., and J. A. Killian. 2003. Protein-lipid interactions studied with designed transmembrane peptides: role of hydrophobic matching and interfacial anchoring. *Mol. Membr. Biol*. 20:271–284.
118. Seddon, J. M., R. D. Kaye, and D. Marsh. 1983. Induction of the lamellar-inverted hexagonal phase transition in cardiolipin by protons and monovalent cations. *Biochim. Biophys. Acta*. 734:347–352.
119. Marsh, D., and J. M. Seddon. 1982. Gel-to-inverted hexagonal ($L_\beta$-$H_{II}$) phase transitions in phosphatidylethanolamines and fatty acid-phosphatidylcholine mixtures, demonstrated by $^{31}P$ NMR spectroscopy and x-ray diffraction. *Biochim. Biophys. Acta*. 690:117–123.
120. Heimburg, T., P. Hildebrandt, and D. Marsh. 1991. Cytochrome *c*-lipid interactions studied by resonance Raman and $^{31}P$ NMR spectroscopy. Correlation between the conformational changes of the protein and the lipid bilayer. *Biochemistry*. 30:9084–9089.
121. Powell, G. L., and D. Marsh. 1985. Polymorphic phase behavior of cardiolipin derivatives studied by $^{31}P$ NMR and x-ray diffraction. *Biochemistry*. 24:2902–2908.
122. King, M. D., and D. Marsh. 1989. Polymorphic phase behavior of lysopalmitoylphosphatidylcholine in poly(ethylene glycol)-water mixtures. *Biochemistry*. 28:5643–5647.
123. Powell, G. L., P. F. Knowles, and D. Marsh. 1990. Incorporation of cytochrome oxidase into cardiolipin bilayers and induction of nonlamellar phases. *Biochemistry*. 29:5127–5132.